REPORT NO. P76-232
HAC REF. NO. D3119
DEPT. REF. 2753/773

Contract N00019-75-C-0160

PHASED ARRAY ANTENNAS SCANNED NEAR ENDFIRE

FINAL REPORT

JANUARY 1975 TO MARCH 1976

Prepared for the AIR SYSTEMS COMMAND
Department of the NAVY

ANTENNA DEPARTMENT

HUGHES

RADAR SYSTEMS GROUP
HUGHES AIRCRAFT COMPANY
CULVER CITY, CA 90230

APPROVED FOR PUBLIC RELEASE:
DISTRIBUTION UNLIMITED

(14) HAC-P76-232, HAC-TIE-D3119

Report No. P76/232
HAC Ref. D3119
Dept. Ref. 2753/773

(6)

PHASED ARRAY ANTENNAS SCANNED NEAR ENDFIRE.

CONTRACT N00019-75-C-0160

(9) FINAL REPORT, Jan 75 — Mar 76,

(11) Mar 76

(12) 67 p.

(10) Prepared by
P. C. Bargeliotes
A. T. Villeneuve
W. H. Kummer
Antenna Department
Radar Microwave Laboratory

(15) N00019-75-C-0160

Prepared for

Air Systems Command
Department of the Navy
Washington, D.C.

Engineering Division

Hughes Aircraft Company - Culver City, California

411 681

12

CONTENTS

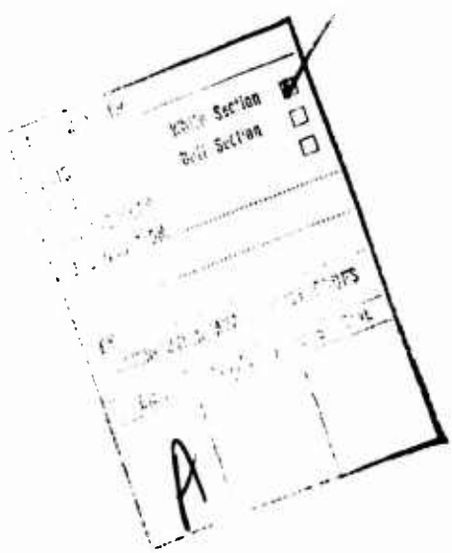

LIST OF ILLUSTRATIONS

ILLUSTRATIONS (Continued)

ACKNOWLEDGMENTS

The following personnel of the Hughes Engineering Division contributed to the Phased Array Antennas Scanned Near Endfire program during the period covered by the contract.

Dr. W.H. Kummer	Program Manager Radar Microwave Laboratory
Dr. P.C. Bargeliotes	Antenna Department
Dr. A.T. Villeneuve	Antenna Department

During this program several technical exchanges occurred between the personnel performing on the program and Drs. A. Hessel (PINY) and R.C. Hansen (consultant). Their suggestions and comments are appreciated.

The technical officer for this program was Mr. J.W. Willis (AIR-310B).

1.0 INTRODUCTION

Excellent agreement has been shown between element patterns of circumferential and radial slots on a cone, computed with the normal mode series computer programs, and patterns measured with an experimental model with both types of slots. When the modal series is used for the computation of exact patterns, the number of modes required for convergence of the series increases as the distance of the slot location from the tip of the cone increases. Computational difficulties from accumulated round-off errors also affect the accuracy and limit the applicability of the modal series program to element positions not too far from the cone tip.

The approximate asymptotic approach, on the other hand, allows the separation of the diffracted field and the geometrical optics field. More specifically, the asymptotic approach resulted in complete expressions for the E_θ and E_ϕ radiation fields in terms of optical, transition, and diffraction fields. The complete expressions for each of the two field components, in a form suitable for numerical computation, were included in the Final Report on Contract No. N00019-74-C-0127.* An examination of these expressions indicates that the diffraction coefficients of both field components are only a function of the angular coordinates and not of the location of the radiating element. The diffraction fields for any element location may then be found by taking the product of these diffraction coefficients and the factor containing the information about the location of the radiating element. The diffraction

*P. C. Bargeliotes, A. T. Villeneuve, and W. H. Kummer, Pattern Synthesis of Conformal Arrays, Final Report on Contract N00019-74-C-0127, Hughes Aircraft Company, January 1974 to January 1975.

coefficients need to be computed only once for a given cone angle, so that the repetition of lengthy computations is eliminated. The optical and transition portions of the fields are given in terms of functions that are more suitable for numerical computation than the modal series expressions.

Because a number of the special functions in these expressions presented considerable numerical computational difficulty, they were investigated individually for a better understanding of their behavior. In the notation of the Final Report referenced previously, these special functions included T(u), U(u), $U_\phi(u)$, and the branch-cut contributions $I^{(1)}_{BR}(\alpha)$ and $I^{(1)}_{BR\phi}(\alpha)$. The subscript ϕ denotes that the function is used only for the ϕ-component of the field. A detailed description of the behavior of these special functions is included in Section 2 of this report. Various plots of optical and transition fields for the first four modes together with certain corrections to the asymptotic expressions are included in Section 3. In Section 4, the diffraction fields and diffraction coefficients are examined in detail.

The diffraction coefficient and the diffraction field for a particular circumferential mode were computed numerically for both polarizations from the approximate expressions. The computation of the diffraction coefficients requires knowledge of the roots of associated Legendre functions as well as of the functions themselves and their derivatives. Computational routines for the roots and the functions are available in the exact modal series program. These routines are made available for the computation of the diffraction coefficients through combination of the asymptotic method program with the exact modal series program. More importantly, the combination of the two computer programs allows pattern computations in the regions in which the asymptotic expressions fail to yield accurate results. As will be seen later, the region of poor performance of the asymptotic method includes the region $\theta \leq \pi - \theta_0$ for the θ-polarization. For the ϕ-polarization, this region is extended even farther. In addition, the asymptotic method is not valid for radiating elements close to the tip of the cone.

Radiation patterns of the circumferential slot for a particular azimuthal mode were computed by a summation of the optical, transition, and diffraction fields for the particular mode. Total radiation patterns were obtained by

summation of sufficient azimuthal modes in a manner similar to that used in the modal series program. In Section 5, total radiation patterns for the first three modes are compared with corresponding patterns from the exact modal series computer program. Also in this section are shown patterns computed from a computer program that combines the asymptotic program with the modal series program.

In Section 6, the results of calculations of mutual coupling between slots located on a circular cylinder are presented in graphical form for various separations.

2.0 NUMERICAL COMPUTATION OF TRANSITION FUNCTIONS

Because each of the special functions considered has an inherent singularity, a computational difficulty results. The validity of the approximations for only a limited range of the particular independent variable further compounds the computational difficulty. For brevity, the notation used in the referenced Final Report (1975) will be followed. Details of the derivation of the functions can be found in Appendix A of the same report.

2.1 ZEROTH-ORDER TRANSITION T(u)

The zeroth-order transition function T(u) is defined by

$$T(u) = \left[f(|u|) + g(|u|) + i\left[f(|u|) - g(|u|)\right] - \frac{1+i}{\pi|u|} \right] \mathrm{sgn}(u) \qquad (1)$$

where $u = (ka/\pi)^{1/2}$ $\alpha = (ka/\pi)^{1/2}(\pi - \theta_o - \theta)$ and the auxiliary functions f, g have simple rational approximations. It is an odd function of u and its singularity is characterized by the last factor in Equation (1). The magnitude and phase variation as a function of u, which is related to θ, is shown in Figure 1. The zeroth-order transition function is used to order $O\left[1/\sqrt{ka}\right]$ in the E_ϕ component and $O\left[1/ka\right]$ in the E_θ component.

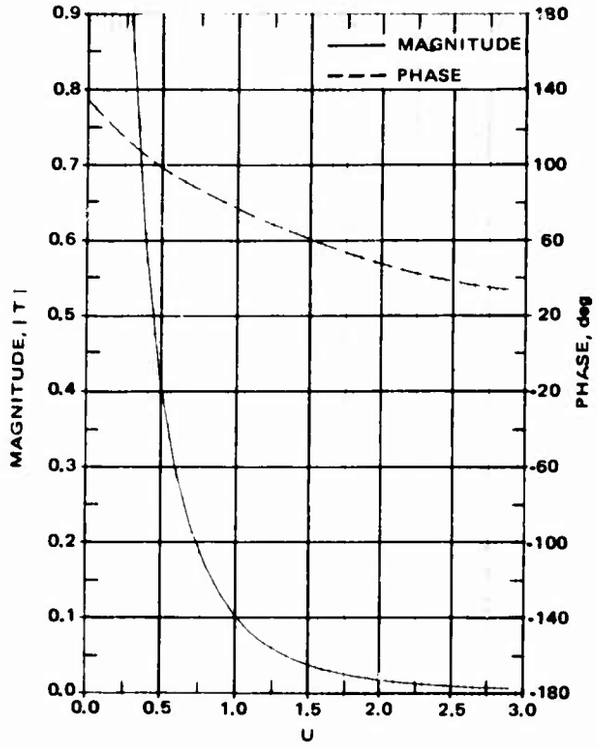

Figure 1. Zeroth-order transition, T(u).

2.2 FIRST-ORDER TRANSITION, U(u)

The first-order transition function is defined by the expression

$$U(u) = \frac{1}{\sqrt{\pi}} \int_{-\infty}^{\infty} \exp(-x^2)\, \mathrm{Ln}(w-x)\, dx - \mathrm{Ln}(w) \qquad (2)$$

where

$$w = \left(\frac{ika}{2}\right)^{1/2} \qquad \alpha = \left(\frac{i\pi}{2}\right)^{1/2} u$$

It can be easily shown that U(u) is an even function of u. From the expression it is evident that U(u) increases very rapidly near u=0 and decreases to zero as u becomes large. Figure 2 shows the magnitude and phase of the function. For $|u|<2.6$, the function was computed with a power series expansion of the

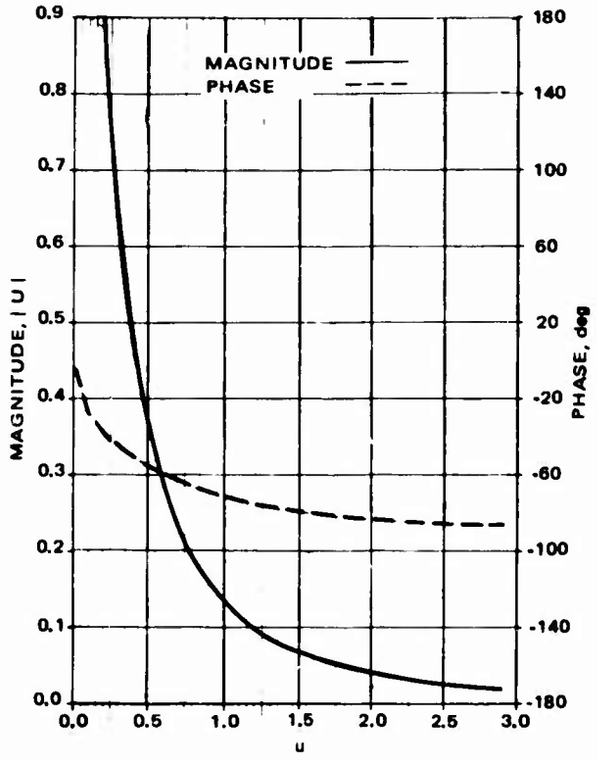

Figure 2. First-order transition, U(u).

integrand and then from the results of the moment theorem of the Gaussian density function. For $|u| \geq 2.6$, the function was computed by an asymptotic expression of the integrand. The transition from one range to the other is excellent, as shown by the graph in Figure 2. The computed values agree to six significant figures at the transition point. This computational technique results in a very accurate and rapid computation of the function.

2.3 FIRST-ORDER TRANSITION FUNCTION, $U_\phi(u)$

The general form of the first-order transition function was found in the analysis for the E_ϕ component and is given by the expression

$$U_\phi(u) = \frac{1}{\sqrt{\pi}} \int_{-\infty}^{\infty} e^{-(x-ib)^2} \, \mathrm{Ln}(w-x)\, dx - \mathrm{Ln}\,(w) \qquad (3)$$

where

$$b = \frac{e^{-i\,\pi/4}}{\sqrt{2\,ka}}$$

From a comparison of Equations (2) and (3), it is evident that $U(u) = \lim_{b \to 0} U_\phi(u)$. The details of the derivation and the evaluation of the integral for both positive and negative values of u are included in Appendix A of the Final Report (1975).

The definition of $U_\phi(u)$ given by Equation (3) also introduced an additional phase factor $e^{i/2ka}$ in the evaluation of the basic contour integral; this factor is neglected because, throughout the analysis, concern is with the computation of the fields to order $O\left[(ka)^{-1/2}\right]$. Unlike U(u), $U_\phi(u)$ is neither an even function nor an odd function of u. Figure 3 shows the magnitude and phase variation of $U_\phi(u)$ for $0 < u < 6$ as computed from computational algorithms similar to those used for the computation of U(u). Both magnitude and phase decrease rapidly as u increases and show only moderate variation for large values of u. The behavior is similar to U(u) for the same range. As u becomes increasingly negative, however, the phase of the function varies moderately. Figure 4 shows $U_\phi(u)$ for $-3 < u < 3$. It is pointed out that, for ka=39, and θ_o=170 degrees, the range of u for which the various first-order transition functions must be computed is approximately $-10.5 < u < 10.5$.

2.4 BRANCH-CUT CONTRIBUTIONS, $I^{(1)}_{BR\,\phi}(\alpha)$, $I^{(1)}_{BR}(\alpha)$

In evaluation of the first-order deformed contour integral that passes through the saddle points, branch cuts were introduced parallel to the imaginary axis for the logarithmic singularities of the integrand. The general

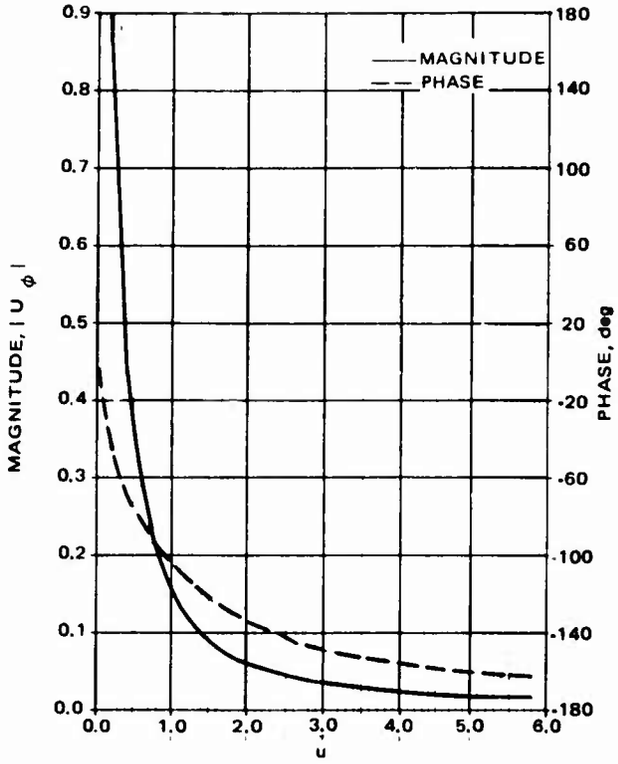

Figure 3. First-order transition, $U_\phi(u)$, $0<u\leq 6$

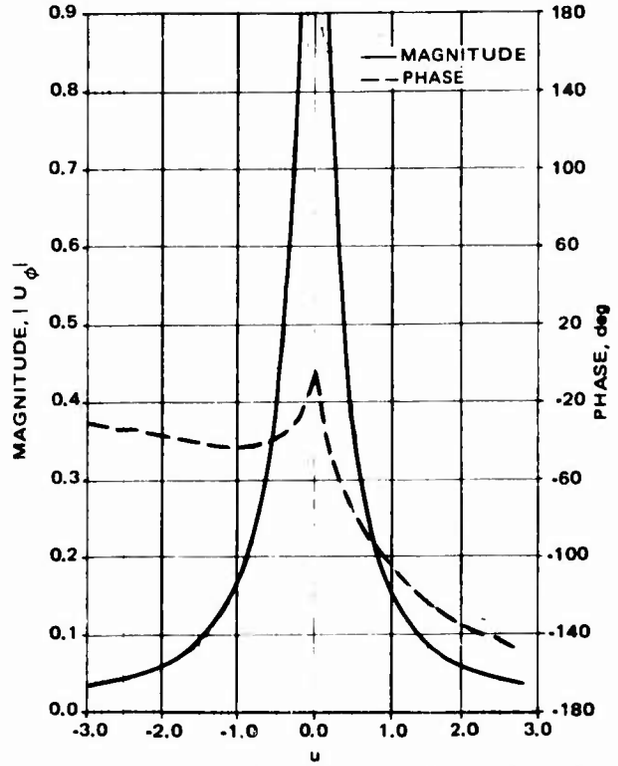

Figure 4. First-order transition, $U_\phi(u)$, $|u|\leq 3$

expression of the branch-cut contribution was derived in Appendix A of the Final Report (1975) and is corrected and repeated here:

$$I^{(1)}_{BR\phi}(\alpha) = \pi i e^{i\left(k a \cos\alpha + \alpha + \frac{ka}{2}\cos\alpha \tan^2\alpha' - \frac{\pi}{4}\right)} \cdot \sqrt{\frac{2\pi}{k a \cos\alpha}}\ \operatorname{erfc}\left(\sqrt{\frac{i\, ka \cos\alpha \tan^2\alpha'}{2}}\right) \tag{4}$$

where $\tan\alpha' = \tan\alpha - \frac{1}{k a \cos\alpha}$. The function $I^{(1)}_{BR}(\alpha)$ that appears in the field expressions of both components is obtained from the above by multiplying by $e^{-i\alpha}$ and taking $\tan\alpha' = \tan\alpha$. In these functions α may take either of the following values:

$$\begin{aligned} \alpha_{10} &= \pi - \theta_o - \theta \\ \alpha_{20} &= \pi - \theta_o + \theta \end{aligned} \tag{5}$$

From the definition it is evident that $\pi - 2\theta_o \le \alpha_{10} \le \pi - \theta_o$ and $\pi - \theta_o \le \alpha_{20} \le \pi$ as θ varies from 0^o to θ_o. Also, $\alpha_{10} = \alpha_{20}$ when $\theta = 0^o$. Because for $\alpha_{10} \le 0$ the branch cut does not lie in the path of integration, $I^{(1)}_{BR}(\alpha_{10})$ and $I^{(I)}_{BR\phi}(\alpha_{10})$ are only considered when $\alpha_{10} > 0$. The first-order branch-cut contributions for α_{10} were computed with Equation (4) for $I^{(1)}_{BR\phi}(\alpha_{10})$ and with the corresponding expression for $I^{(1)}_{BR}(\alpha_{10})$. The results are shown in Figure 5. The magnitude of both functions decreases as α_{10} increases, while the phase shows moderate variation with increasing α_{10}. This result is true at least for the range of α_{10} indicated here. Any smaller values of α_{10} fall outside the range of interest and the functions were not considered.

The expression in Equation (4) is unsuitable for computation for α_{20} near $\pi/2$, because of the $1/\cos\alpha$ factor. An asymptotic form of Equation (4) with the asymptotic representation of the complementary error function, permits computations at and near $\pi/2$. A transition point of $\left|\alpha_{20} - \pi/2\right| = 0.53$ radian was selected for the two different computational algorithms; the results are shown in Figure 6 for both $I^{(1)}_{BR\phi}(\alpha_{20})$ and $I^{(1)}_{BR}(\alpha_{20})$. The magnitude of

a. $I^{(1)}_{BR\,\phi}$

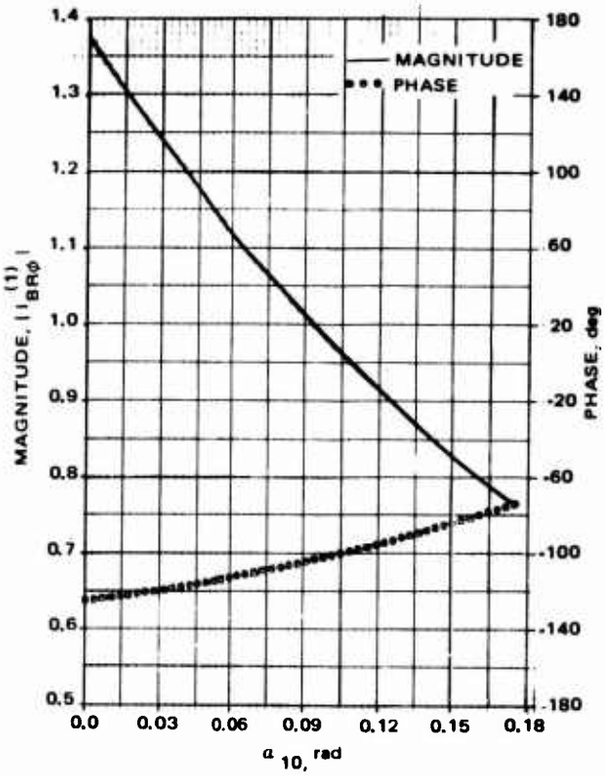

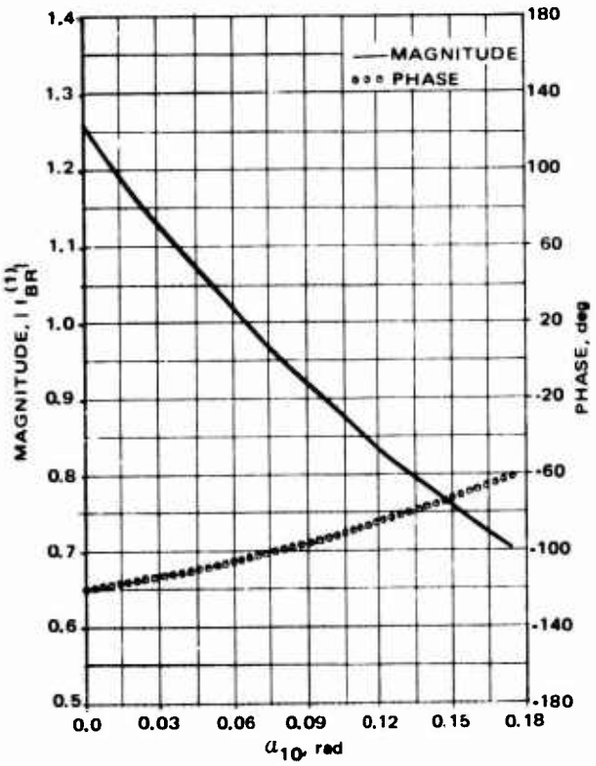

b. $I^{(1)}_{BR}$

Figure 5. Branch-cut contributions for α_{10}.

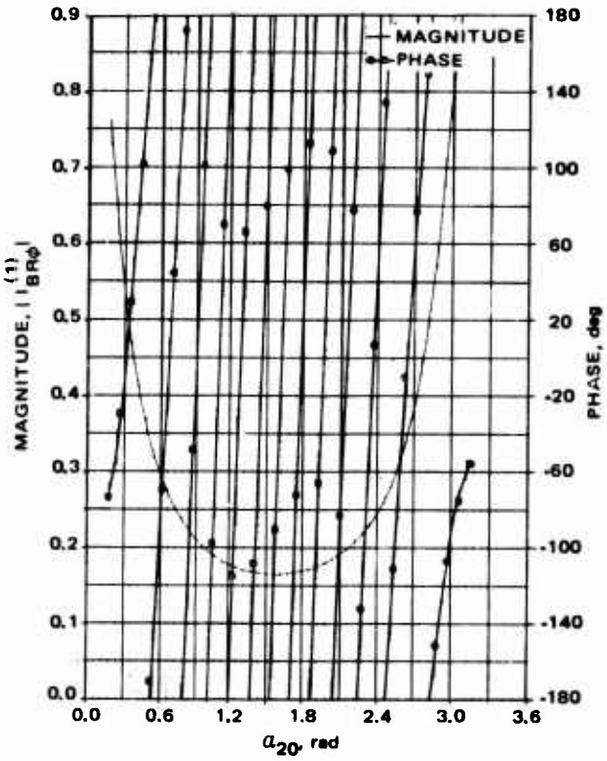

a. $I^{(1)}_{BR\ \phi}$

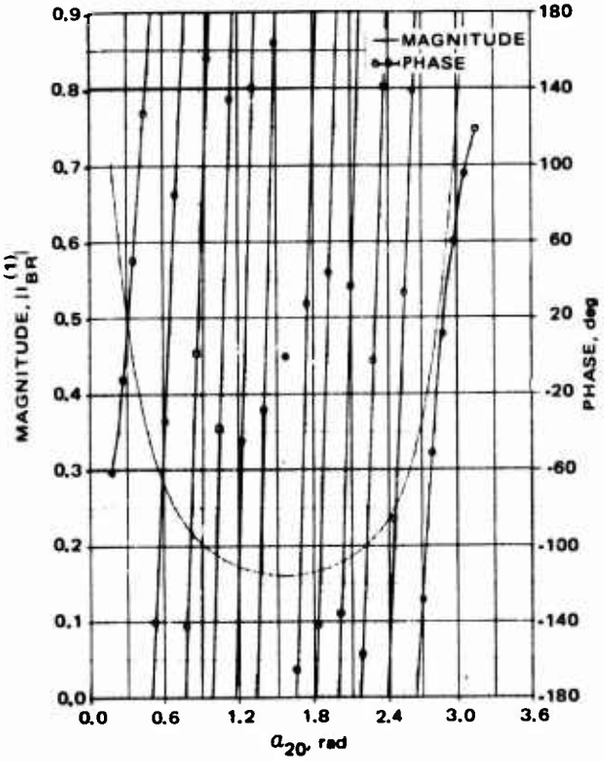

b. $I^{(1)}_{BR}$

Figure 6. Branch-cut contributions for α_{20}.

both functions increases rapidly and at about the same rate as α_{20} approaches π and $\pi-\theta_o$. Both functions exhibit rapid variation in phase, as shown by the curves.

The branch-cut contributions, $I^{(1)}_{BR\phi}(\alpha_{10})$ and $I^{(1)}_{BR\phi}(\alpha_{20})$, were also computed with $\tan \alpha' = \tan \alpha$ in Equation (4). The changes in the magnitude and phase of the functions are noticeable throughout the range of α but are more so when α is near 0 and π. In view of this result, it is concluded that the complete expression of Equation (4) should be used in the computation of the branch-cut contributions.

3.0 NUMERICAL COMPUTATION OF OPTICAL AND TRANSITION FIELDS

The formal expressions of the θ- and ϕ-components of the electric fields of a circumferential slot on a conducting cone are given in the prior Final Report (1975) and will not be repeated here.*

The various terms in the field expressions were grouped together with the proper coefficients in a way that makes the optical, transition, and diffraction fields easily identifiable. This arrangement allows for easy comparison between the different types of fields of the θ- and ϕ-polarizations. All computations were performed for a particular mode, paralleling the normal mode series computer program. In the subsections that follow, the discussion centers mostly on the $m = 1$ mode because it is the lowest order mode of the ϕ-polarization. The $m = 0$ mode is only applicable to the θ-polarization.

---

*Bargeliotes, Villeneuve, Kummer, op. cit. The following typographical errors should, however, be corrected:

1. The coefficients n_1, n_2 in Equation (47c), p. 13, should be η_1, η_2.
2. The second exponential of Equation (3.5), p. 20, should be $e^{-ika \cos(\theta_o + \theta)}$.
3. The radical in the last factor of Equation (3.6), p. 22, should be $\sqrt{2\pi/ka}$.
4. The coefficient of the second bracketed factor of Equation (3.17), p. 25, should be $i/\sin\theta_o$.
5. The coefficient i of Equation (3.22), p. 26, should be deleted.
6. The brace ($\}$) should be included at the end of the TF_ϕ expression of Equation (3.22), p. 27.
7. The $\sigma_{m\phi}(\theta, \theta_o)$ expression of Equation (3.22), p. 27, should be multiplied by -1.

For convenience, the different types of fields for the m^{th} mode are identified by the name used in the computer program:

OPM – optical field of θ-polarization (first two terms of $\mathscr{E}_\theta$ expression, p. 13 of Final Report (1975))

OPF – optical field of φ-polarization (first two terms of Equation (3.5), p. 20 of Final Report (1975))

TFT – transition field of θ-polarization (TF term of $\mathscr{E}_\theta$ expression, p. 13 of Final Report (1975))

TFF – transition field of φ-polarization (TFφ term of Equation (3.22), p. 26, and third term of Equation (3.5), p. 20 of Final Report (1975))

DFT – diffraction field of θ-polarization (last term of $\mathscr{E}_\theta$ expression, p. 13 of Final Report (1975))

DFF – diffraction field of φ-polarization (last term of $\mathscr{E}_\phi$ expression, Equation (3.22), p. 26 of Final Report (1975))

These descriptions and page references refer to the Final Report cited above.

3.1 THE OPTICAL FIELD

The optical fields of the θ-component were computed for the lowest four modes and are shown in Figure 7. The magnitude of the optical field is independent of ka and exhibits a singularity of $\theta = 0^o$, while the phase varies rapidly with the angle θ. In these plots, as well as in the plots of the transition fields of the next section, no attempt was made to connect the phase points, as the phase of these fields fluctuates very rapidly through many cycles as a function of θ. All asymptotic modal fields computed for the optical field decrease to a minimum at broadside and increase again near $\theta = 0^o$.

For the φ-polarization, the first contributing mode is the $m = 1$ mode. Furthermore, in a comparison of the analytic expressions of E_θ and E_ϕ, it is evident that the magnitude of the optical field of the φ-polarization is proportional to 1/ka. Because of this difference in the proportionality factor, the optical field of the φ-polarization was at first considered negligible and was not included in the computations. When the optical field was compared with certain factors of the transition field of the same polarization, however, it was found to make significant contributions to the total field. (The overall

a. For m = 0 mode

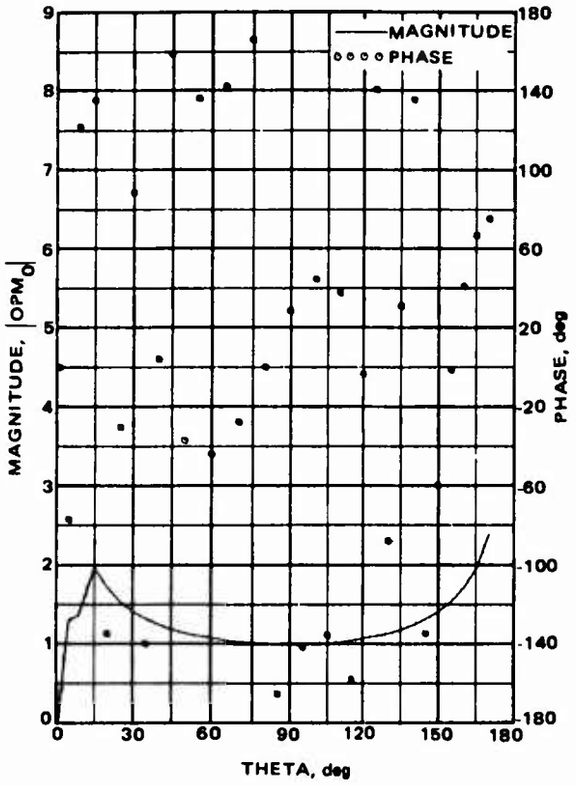

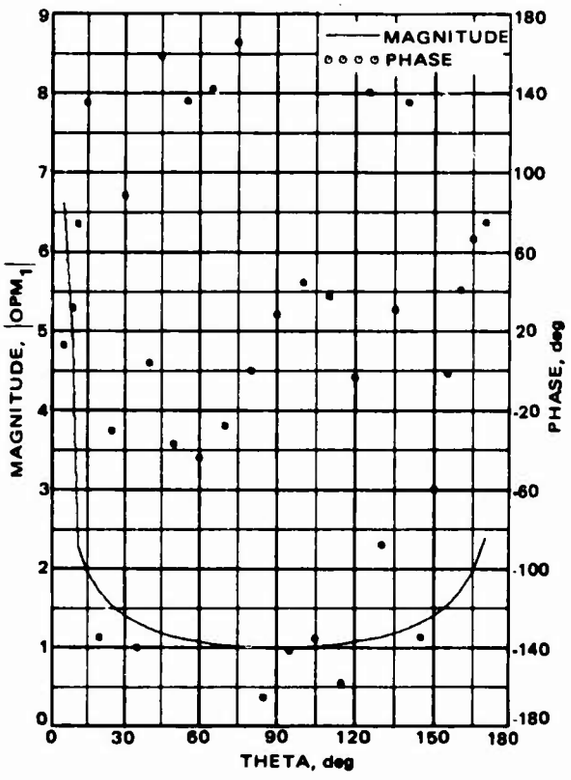

b. For m = 1 mode

(continued)

Figure 7. Computed θ-polarized optical fields for four modes.

c. For m = 2 mode

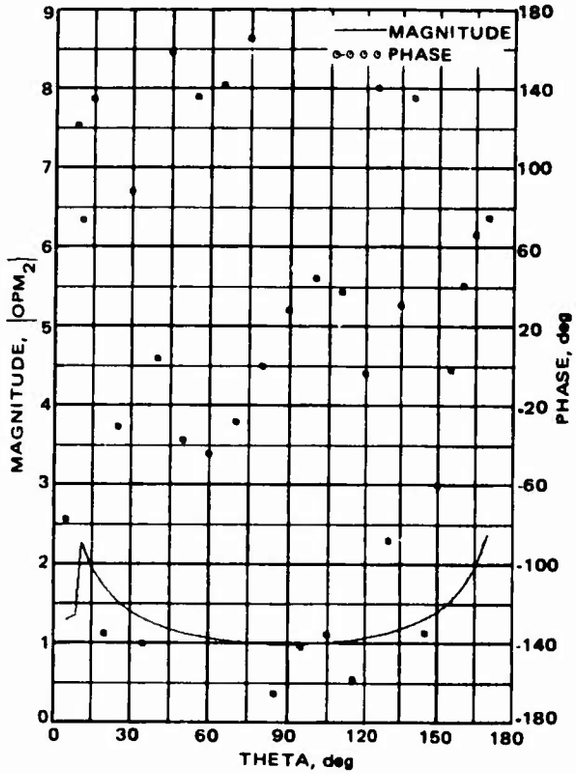

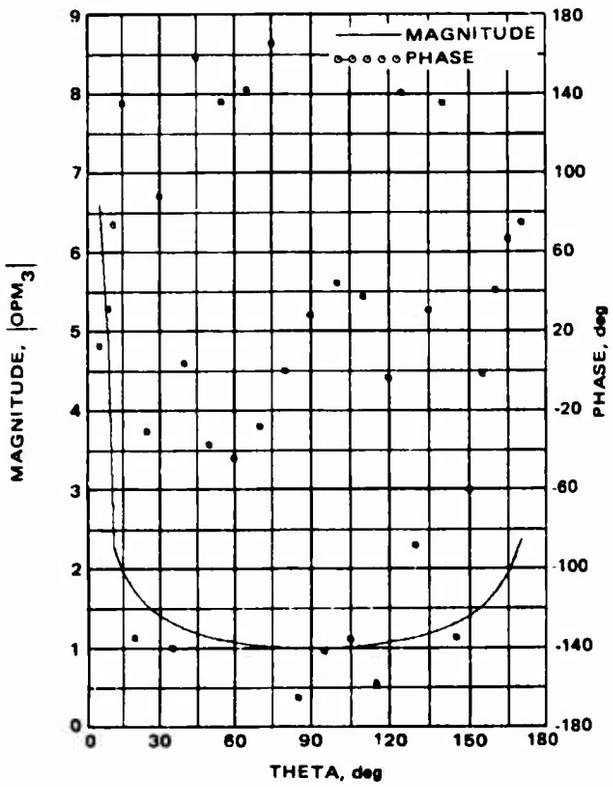

d. For m = 3 mode

(concluded)

Figure 7. Computed θ-polarized optical fields for four modes.

effect of this optical field are covered in the discussion of the computed radiation patterns.) Figure 8a shows this optical field for the m = 1 mode. The factor for the m = 2 mode, shown in Figure 8b, behaves in a similar manner, but its magnitude is at a slightly higher level than the corresponding factor for the m = 1 mode. Even more significant is the contribution of the optical field of the ϕ-polarization for the m = 3 mode (Figure 8c).

3.2 THE TRANSITION FIELD

The transition field of both field components is a much more complicated function, because it is comprised of several special functions such as the zeroth order transition, the first-order transition, and the branch-cut contributions. These special functions were individually investigated and computed previously. For the θ-component, all the special function factors of the total transition field are proportional to $(1/ka)^{1/2}$. Figure 9 presents the modal transition fields of the θ-component for the first four modes. All modes behave similarly in the broadside region but differ significantly at regions near the optical boundary, $\theta = \theta_o$ and $\theta = \pi - \theta_o$.

The transition field of the ϕ-polarization is comprised of several additional factors compared with the transition field of the θ-polarization; it includes branch-cut contributions and first-order transition functions unique to this polarization, in addition to the functions appearing in the θ-polarization expression. These are identified by the subscript "ϕ" in the defining expression. Unlike the θ-polarization, the zeroth-order transition field represented by the $T(u_{10})$ function is of order one in (1/ka) in this component. The significance of this factor can be seen from a comparison of the two graphs in Figure 10; the zeroth-order transition field is included in Figure 10a but not in Figure 10b. The effect of the zeroth-order transition is even more apparent when the approximate modal pattern is compared with the corresponding pattern computed by the normal mode series method. The inclusion of the first-order transition functions, $U_\phi^*(u_{20})$ and $U_\phi^*(u_{30})$, in the computation of the total transition field introduces undesirable oscillations in the magnitude of this field. The exact reason for this degradation is not understood at this time, but it may be caused by improper computation of the two functions. For the present, these factors were omitted from the computations.

a. For m = 1 mode

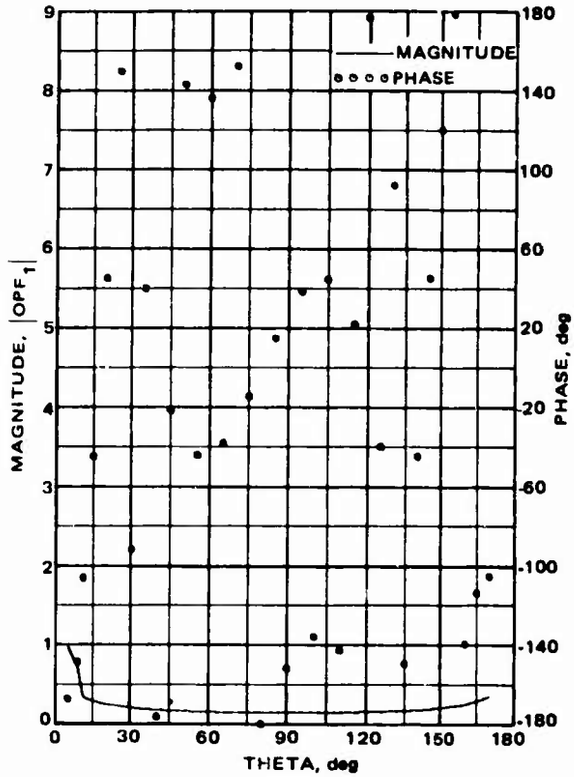

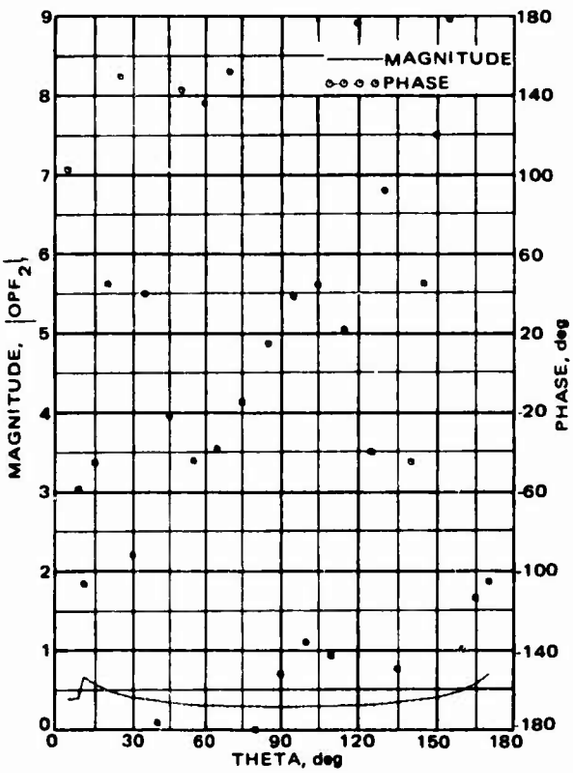

b. For m = 2 mode

(continued)

Figure 8. Computed ϕ-polarized optical fields for three modes.

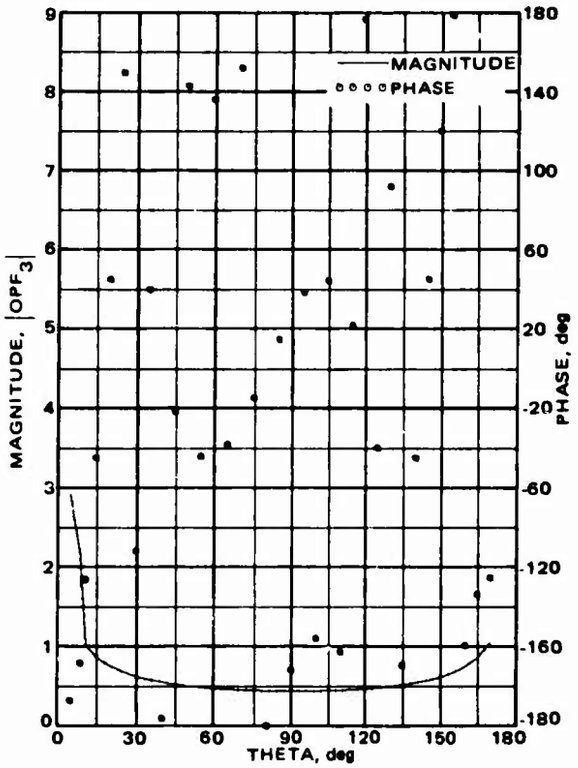

c. For m = 3 mode

(concluded)

Figure 8. Computed ϕ-polarized optical fields for three modes.

a. For m = 0 mode

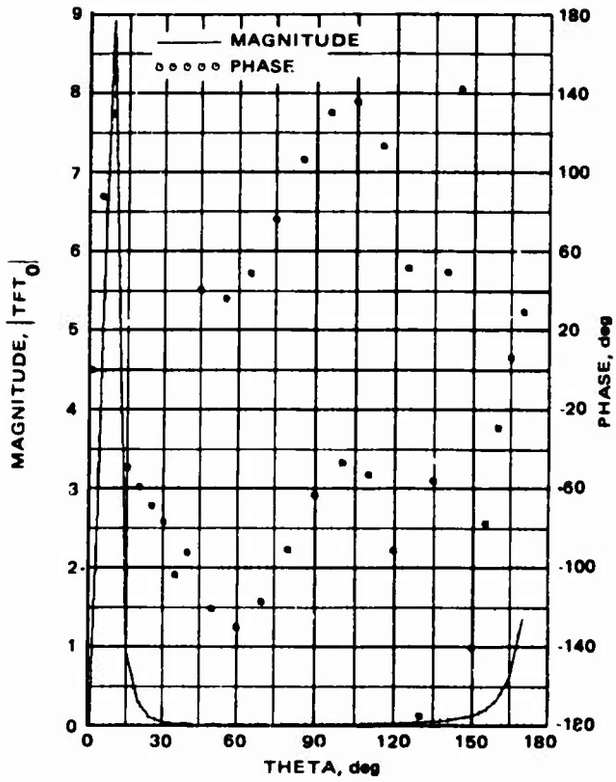

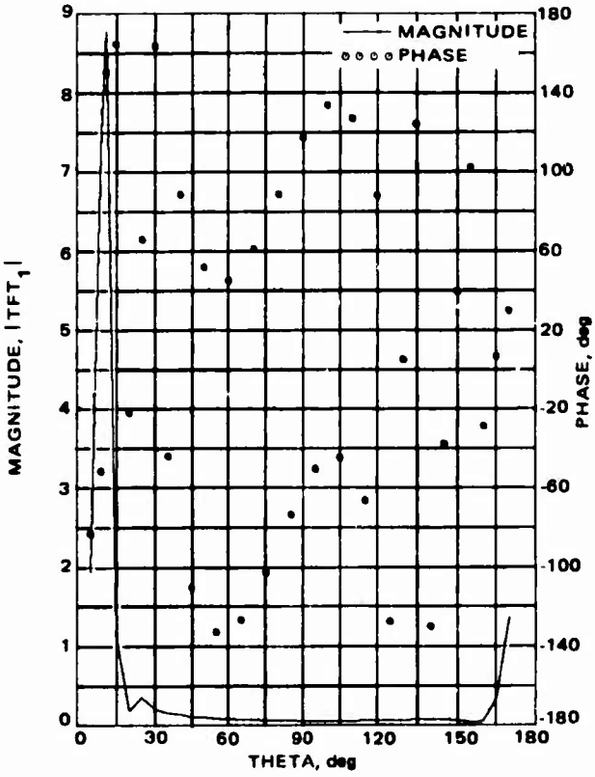

b. For m = 1 mode

(continued)

Figure 9. Computed θ-polarized transition fields for four modes.

c. For m = 2 mode

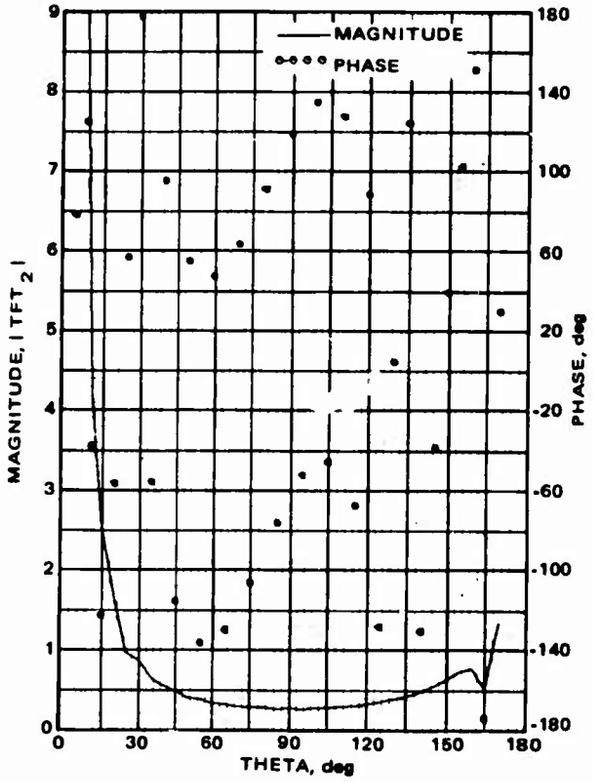

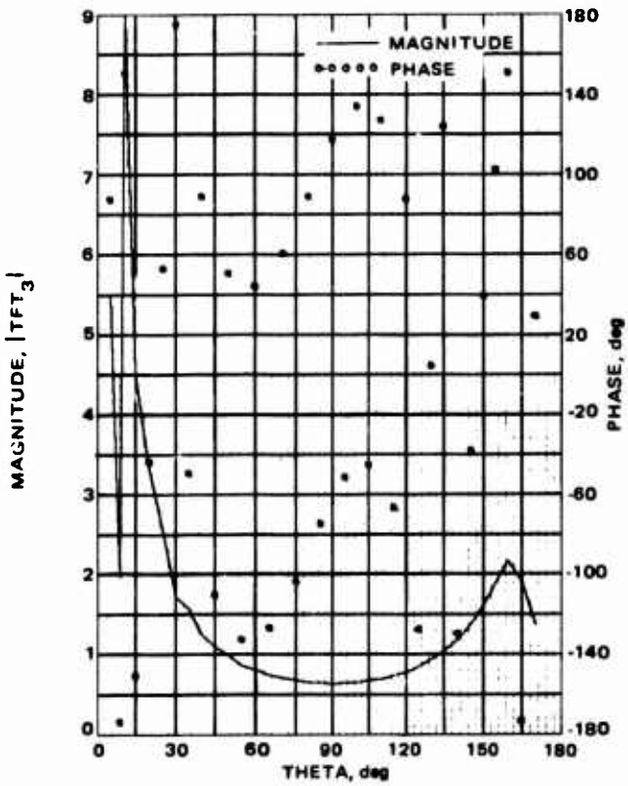

d. For m = 3 mode

(concluded)

Figure 9. Computed θ-polarized transition fields for four modes.

a. Including zeroth-order transition

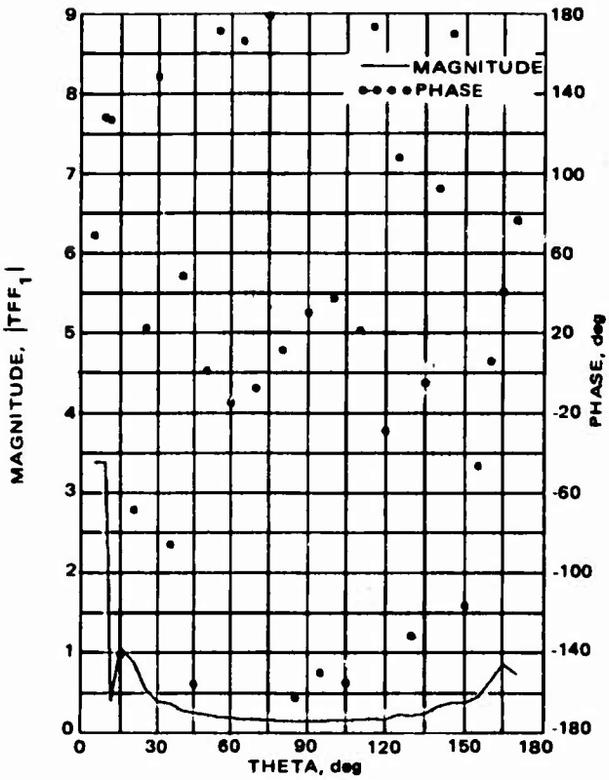

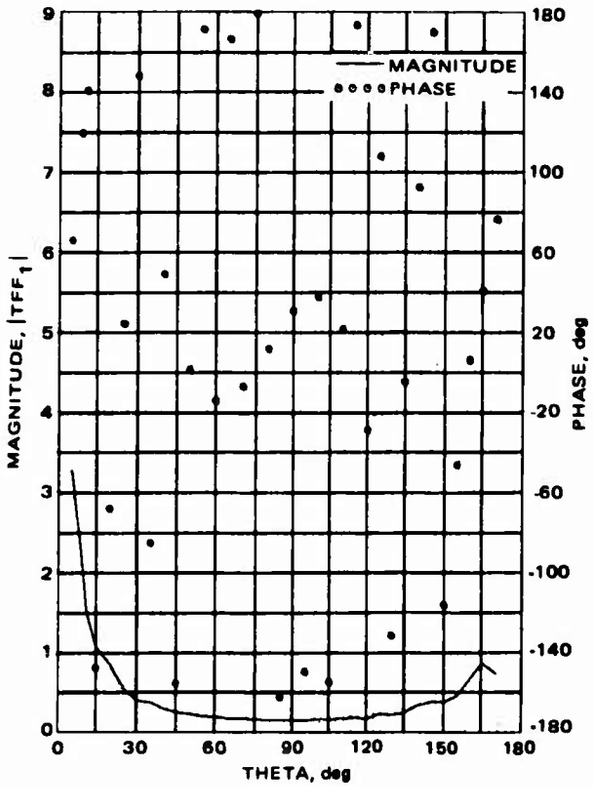

b. Excluding zeroth-order transition

Figure 10. Computed ϕ-polarized transition fields for m = 1 mode

3.3 HIGHER ORDER IN (1/ka) TRANSITION FIELD

The need to include the optical term and the zeroth-order transition term in the total field, both of which are of order 0 (1/ka), prompted the investigation of other terms also of order 0 (1/ka) that had previously been neglected in the field expression. These additional terms arise from the $P^{(1)\ (A)}_{2\phi c_i}$ contour integral, which was set equal to zero in Equation (3.7) of the Final Report (1975). A closed-form expression of this contour integral is

$$P^{(1)\ (A)}_{2\phi\, c_i} = \frac{i}{4\pi^2}\left(\frac{\sin\theta_o}{\sin\theta}\right)^{1/2} \Big\{\Gamma[c_1 + ic_2 + ic_3]I^{(1)}_{BR}(\alpha_{10})H(\alpha_{10})$$

$$+ [c_1 + ic_2 - ic_3]I^{(1)}_{BR}(\alpha_{20})$$

$$- \Gamma[c_1 + ic_2 + ic_3]\sqrt{\frac{2\pi}{ka}}\exp(i(ka - \pi/4))U(u_{10})$$

$$+ 2i(c_3 - c_2)\sqrt{\frac{2\pi}{ka}}\exp(-i(ka - \pi/4))U^*(\bar{u}_{20})\Big\} \qquad (6)$$

where

$$c_1 = \frac{1}{2ka}$$

$$c_2 = \frac{3 + 4m^2}{8ka}\cot\theta_o$$

$$c_3 = \frac{3 + 4m^2}{8ka}\cot\theta$$

All other parameters have the same definition as in the Final Report (1975).

Figure 11 shows the complete transition field with the contour integral contribution included and omitted. From the curves, it is evident that this higher order 1/ka term of the transition field changes the magnitude of the field in the transition regions and the phase at the broadside region. The

a. Including $P_{2\phi ci}^{(1)(A)}$ contribution

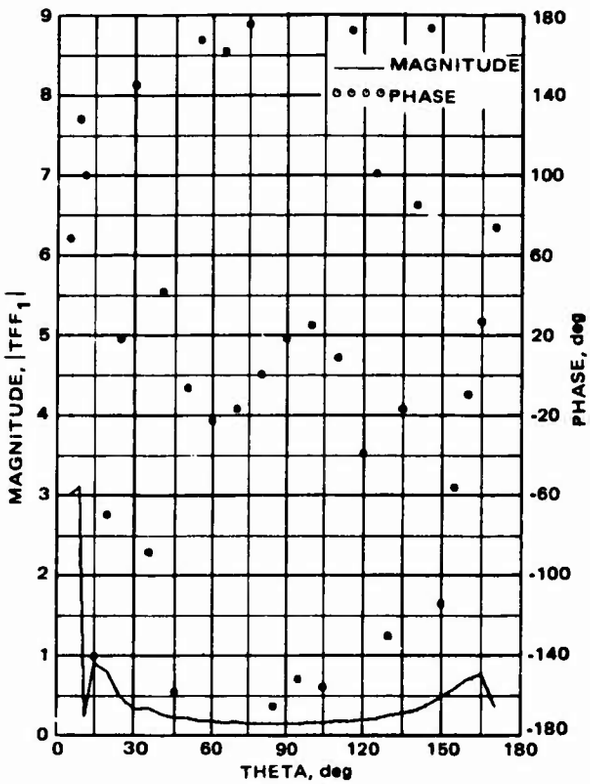

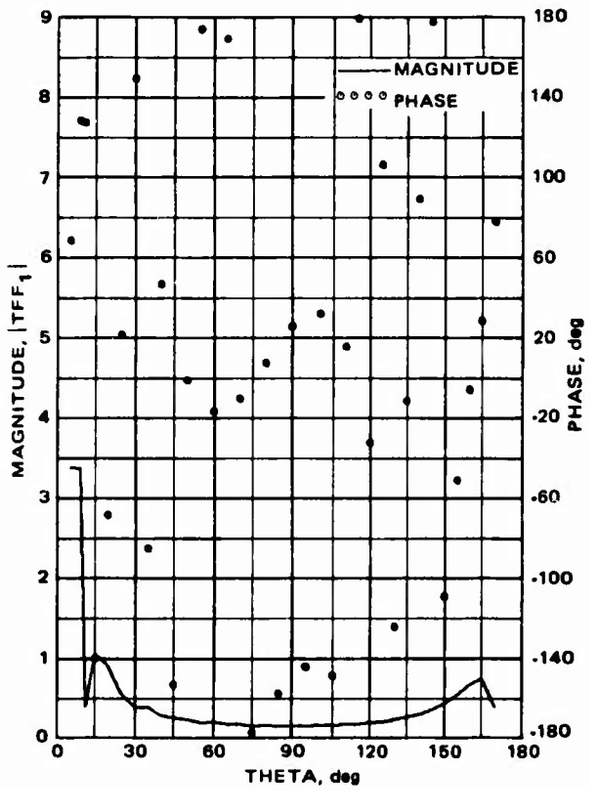

b. Excluding $P_{2\phi ci}^{(1)(A)}$ and $U_{\phi}^{*}(\bar{u})$ contributions

Figure 11. Computed ϕ-polarized transitions fields for m = 1 mode and various contributions.

effect of this term will be best determined by computation of the far-field pattern and a comparison of the computed pattern with the corresponding pattern from the normal mode series.

Transition fields for higher order modes for the ϕ-polarization are shown in Figure 12 for m = 2 and m = 3. These graphs also include the contributions of the $U^{*}_{\phi}(\bar{u}_{20})$ and $U^{*}_{\phi}(\bar{u}_{30})$ functions but not the contour integral $P^{(1)(A)}_{2\phi c_i}$. Again, the transition fields exhibit the singularity at the transition point with rapid phase variation everywhere.

It is apparent from the graphs that the magnitude of the modal transition fields for both components increases as the mode number increases. This behavior of the transition fields, and also of the diffraction fields of the next section, results from the asymptotic representation of the associated Legendre functions:

$$P^{-m}_{\nu-1/2}(\cos\theta) = \left(\frac{2}{\pi \sin\theta}\right)^{1/2} \nu^{-m-1/2} \left(\sin\psi - \frac{1-4m^2}{8\nu} \cot\theta \cos\psi\right) \quad (7)$$

where

$$\psi = \nu\theta + (1-2m)\,\pi/4$$

Equation (7) shows that functions decrease rapidly with m because of the coefficient $\nu^{-m-1/2}$, and at first glance, the transition and diffraction fields should also be decreasing accordingly. The actual expressions for these component fields, however, involve the ratio of the Legendre functions to their derivatives, and the coefficient $\nu^{-m-1/2}$ is eliminated. The ratio is then expanded in a series, with the assumption that

$$\left|\frac{1-4m^2}{8\nu} \cot\theta_o \cos\psi_o\right| \ll \left|\sin\psi_o\right|$$

or that

$$\left|\frac{3+4m^2}{8\nu} \cot\theta_o \sin\psi_o\right| \ll \left|\cos\psi_o\right|$$

a. For m = 2 mode

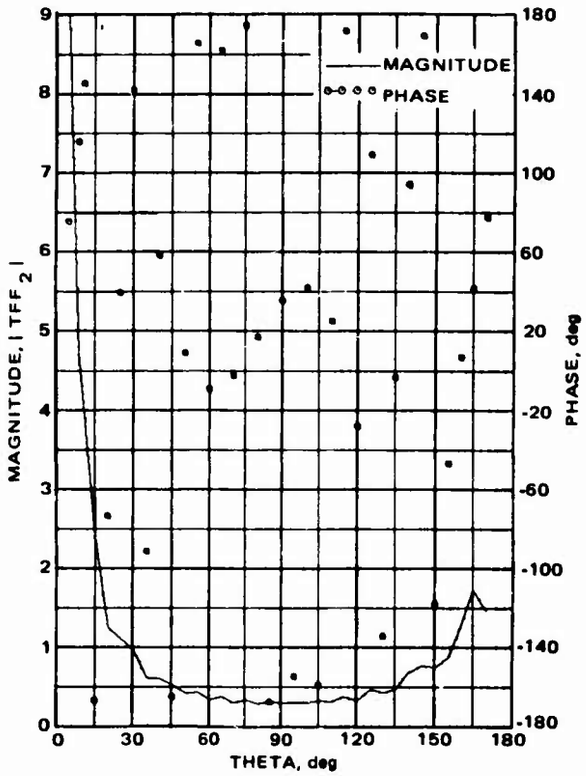

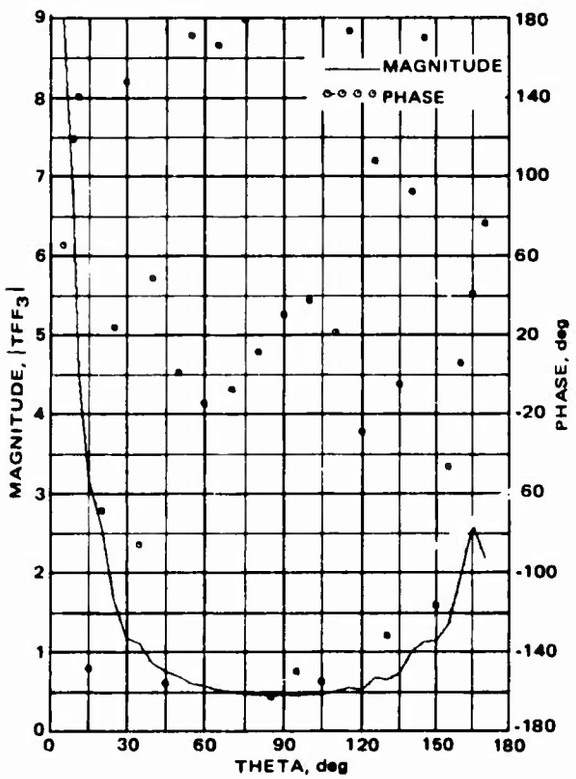

b. For m = 3 mode

Figure 12. Computed ϕ-polarized transition fields for two modes.

These conditions are not always satisfied, and the expansions result in erroneous numerical results, especially for the larger values of m. The possibility of avoiding the series expansion and, thereby, of removing this source of error should be considered.

4.0 NUMERICAL COMPUTATION OF DIFFRACTION COEFFICIENTS AND DIFFRACTION FIELDS

The diffraction field of a particular circumferential mode is a function of a ka-dependent factor and the diffraction coefficient corresponding to the mode in question. The diffraction coefficient is independent of ka, i.e., the position of the radiating element on the conical surface. It is this characteristic of the diffraction coefficient that makes the asymptotic method useful for computation of far-field patterns from radiating elements on a conical surface.

Throughout this report, the diffraction fields of a particular mode are referred to by the computer program variable names for the θ-polarization and ϕ-polarization, DFT and DFF, respectively. The analytical expression of these fields and of the diffraction coefficients, as well as of the optical and transition fields, were given in previous reports on this contract and are identified in Section 3. Computed total diffraction coefficients of the first four modes of the θ-polarization are shown in Figure 13. The corresponding modal diffraction fields are obtained by multiplying the diffraction coefficients by the factor $\exp(ika)/(ka)^{1/2}$. The modal far-field is obtained by adding the diffraction field to the corresponding modal optical and transition fields. The diffraction coefficients of the ϕ-polarization for m=1, m=2, and m=3 modes are shown in Figure 14.

In the computations for the plots of Figures 13 and 14, at least 64 terms were used in the summation of the ΣS_{1n} and ΣS_{2n} series. Figure 15 shows the diffraction coefficients of E_θ and E_ϕ, respectively, of the m=1 mode with only 39 terms in the summation of the two series. Comparison of these curves with the corresponding curves of Figures 13b and 14a, in which 66 terms were used in the series, shows that the magnitude of the functions is

a. For $\sigma_{0\theta}(\theta, \theta_0)$, m = 0

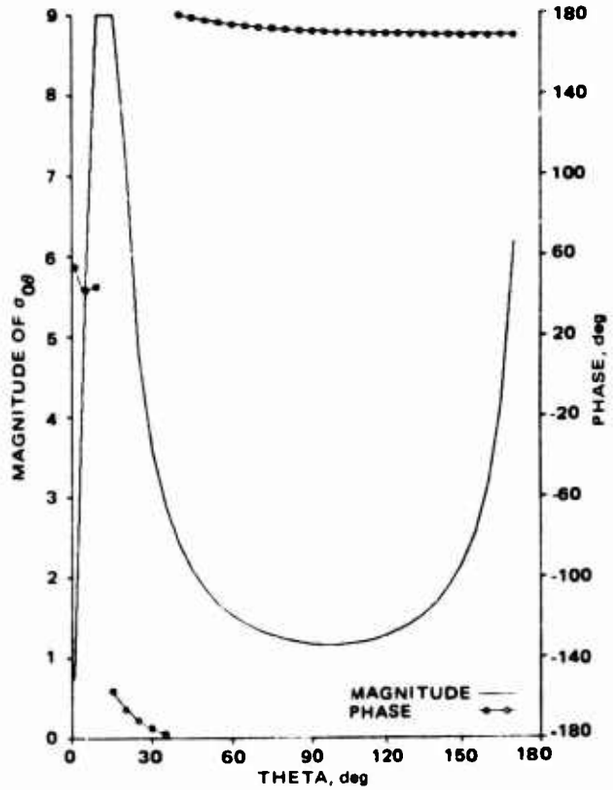

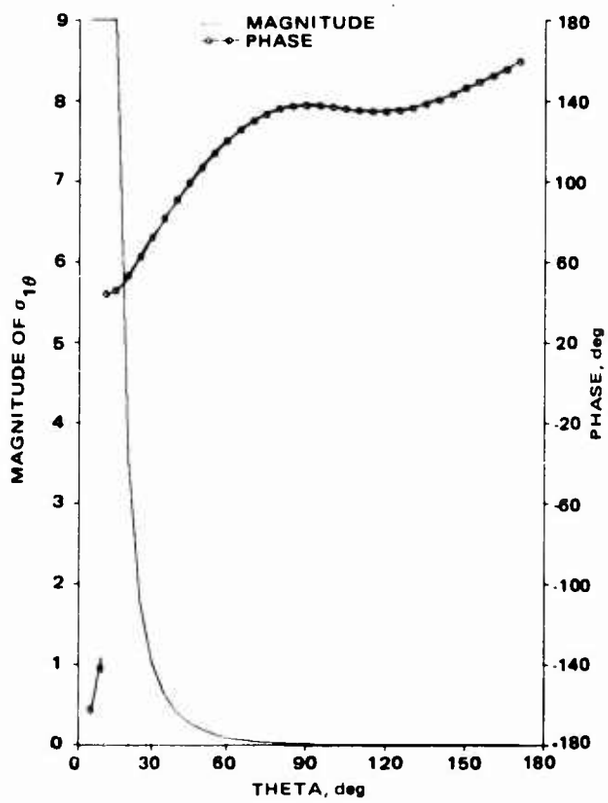

b. For $\sigma_{1\theta}(\theta, \theta_0)$, m = 1

(continued)

Figure 13. Computed diffraction coefficients of θ-polarization for first four modes.

c. For $\sigma_{2\theta}(\theta, \theta_0)$, m = 2

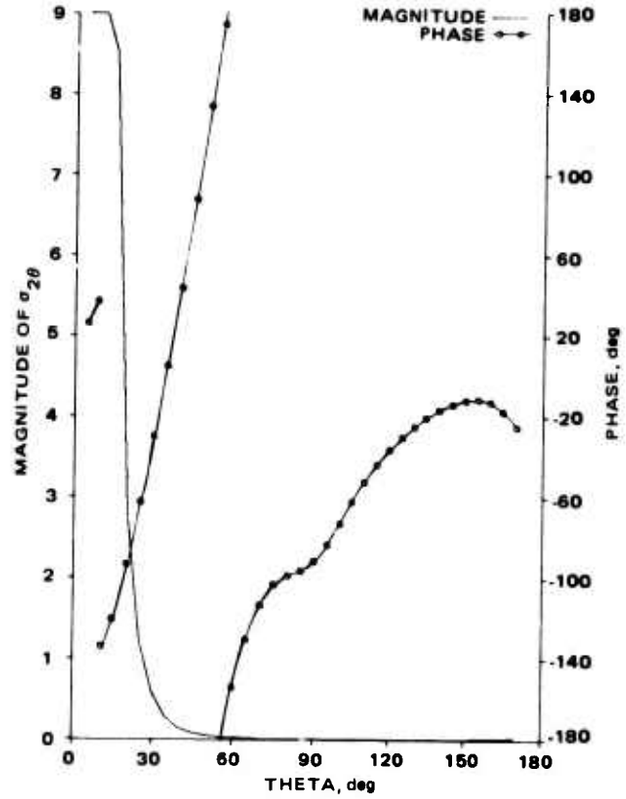

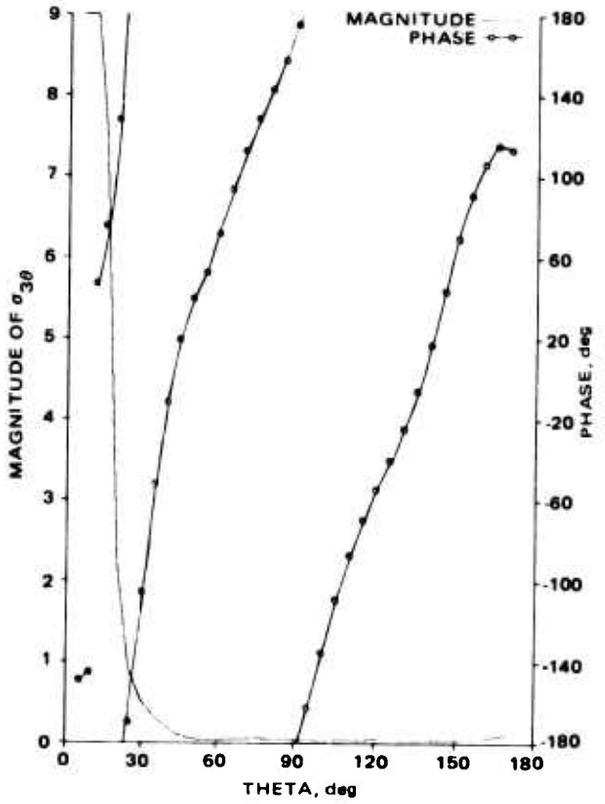

d. For $\sigma_{3\theta}(\theta, \theta_0)$, m = 3

(concluded)

Figure 13. Computed diffraction coefficients of θ-polarization for first four modes.

a. For $\sigma_{1\phi}(\theta, \theta_0)$, m = 1

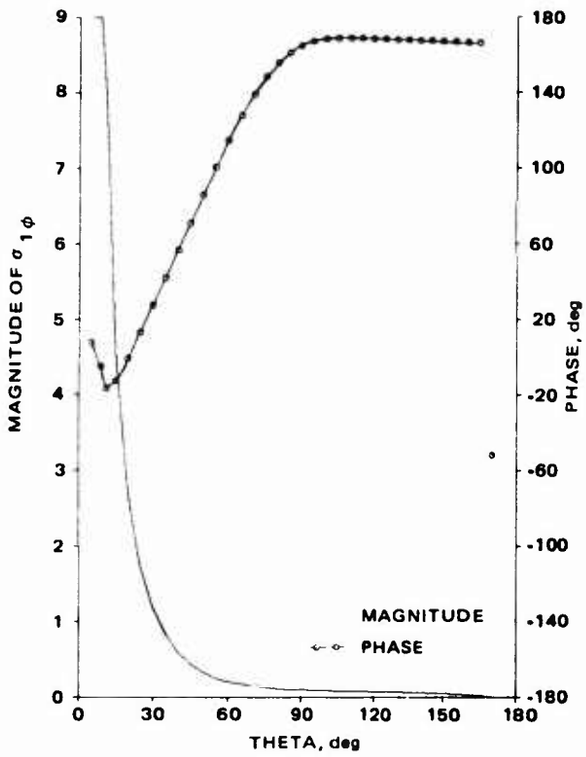

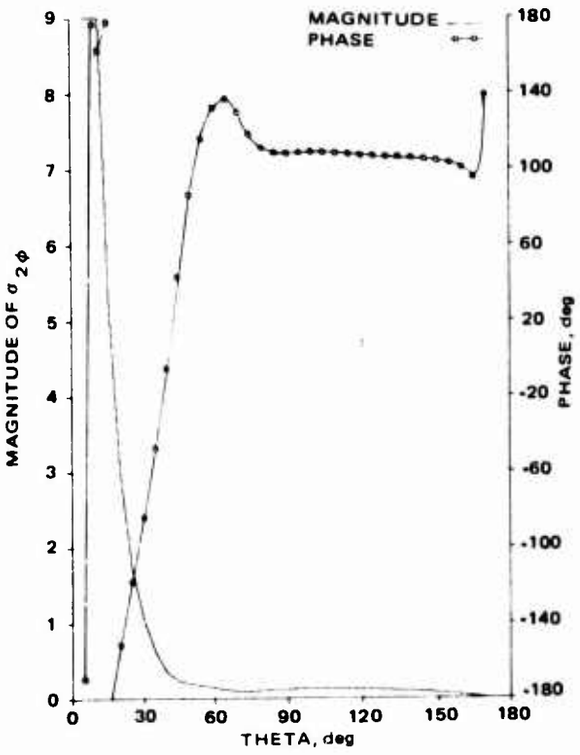

b. For $\sigma_{2\phi}(\theta, \theta_0)$, m = 2

(continued)

Figure 14. Computed diffraction coefficients of ϕ-polarization for first three modes.

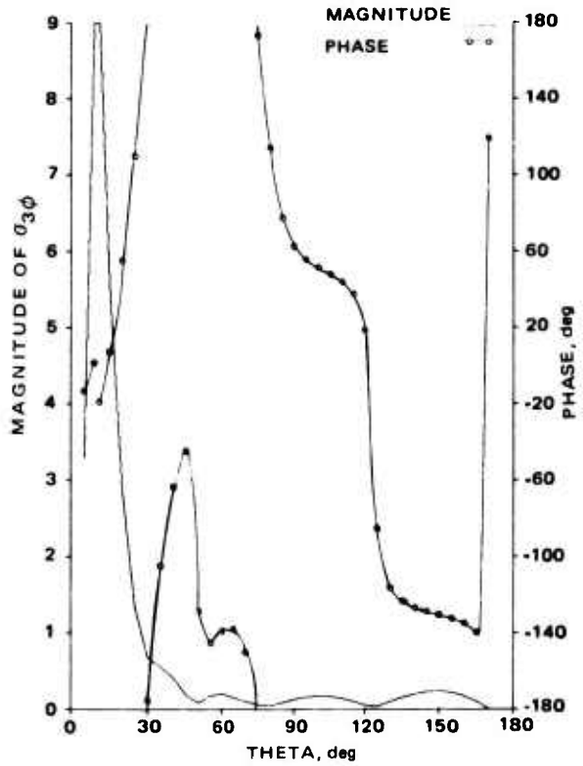

c. For $\sigma_{3\phi}(\theta, \theta_0)$, m = 3

(concluded)

Figure 14. Computed diffraction coefficients of ϕ-polarization for first three modes.

a. For θ-polarization

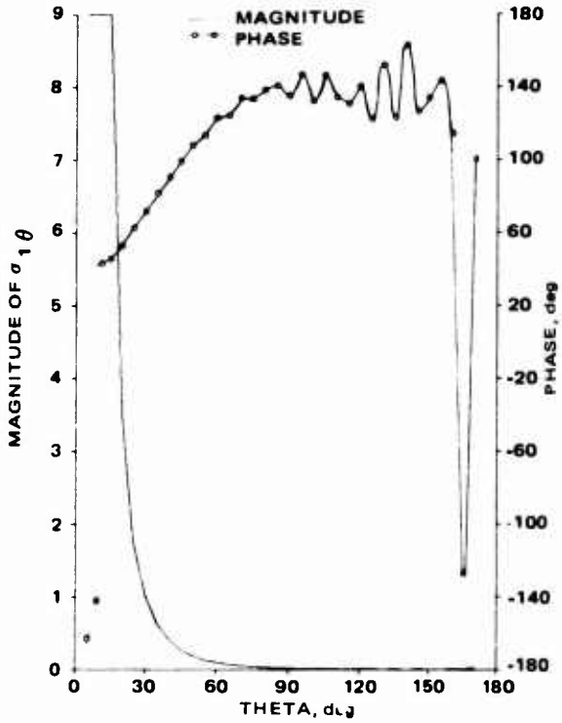

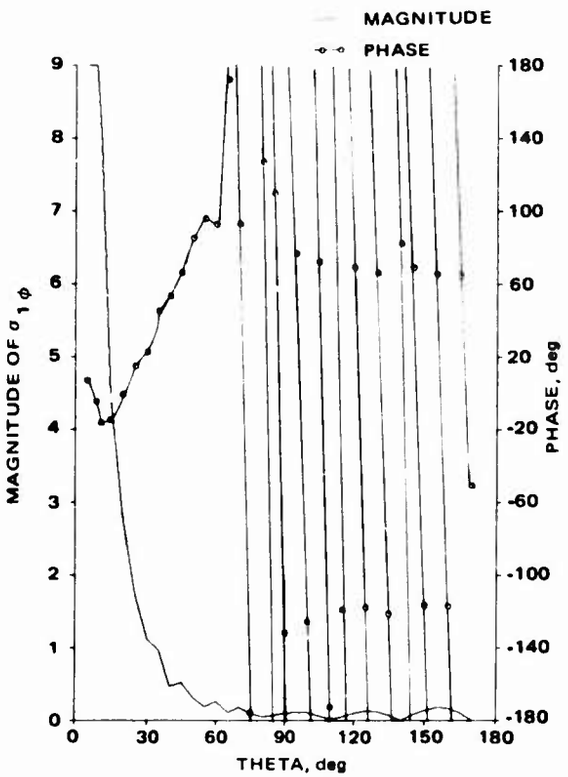

b. For ϕ-polarization

Figure 15. Computed diffraction coefficients of E_θ and E_ϕ for m=1 mode and 39 terms in ΣS_n.

virtually unaltered while the phase variation changes noticeably. Moreover, the difference between the two corresponding graphs is not near the transition point $\theta = \pi - \theta_0$ as suggested by Pridmore-Brown* but rather at angles of θ greater than 60 degrees. Figure 15b demonstrates the overall convergence characteristics of the series in the $\sigma_{m\phi}(\theta, \theta_0)$ diffraction coefficient of the ϕ-polarization with ka terms in the ΣS_{1n}, ΣS_{2n} sums. In all the above computations, ka = 39. This value of ka allows comparison of the computational results with the results from the modal series computer program. Modal patterns showing the effect of the number of terms in the series are presented in the next section. The oscillatory behavior of the magnitude of the diffraction coefficient, $\sigma_{m\phi}(\theta, \theta_0)$, over most of the θ-range and the rapid phase variation are clearly an indication of poor convergence with the indicated number of terms. Comparison of this curve with the corresponding curve of the θ-polarization (Figure 15a) shows that the ϕ-polarization computations are more dependent on the number of terms in the two series ΣS_{1n} and $\Sigma S_{2n\phi}$.

It is also evident from the figures that the diffraction coefficients of the θ-polarization decrease in magnitude with increasing mode number m for the lower order modes, except in the transition regions. The inherent singularity of the diffraction coefficients at $\theta = \pi - \theta_o$ is clearly shown. As the mode number increases, however, the diffraction coefficients of both polarizations increase in magnitude throughout the whole range of the angle theta. The diffraction coefficient of E_θ for m=9, shown in Figure 16, demonstrates this behavior. The increase in magnitude of the diffraction coefficients is believed to be caused by the asymptotic representation of the associated Legendre functions, which results in an incorrect representation of the modal diffraction fields not only in the region $\theta < \pi - \theta_o$ but also in the range $\theta > \pi - \theta_o$.

---

*D. C. Pridmore-Brown, "Diffraction Coefficients for a Slot Excited Conical Antenna," IEEE Trans. on Antennas and Propagation, Vol. AP-20, No. 1, pp. 40-49, January 1972.

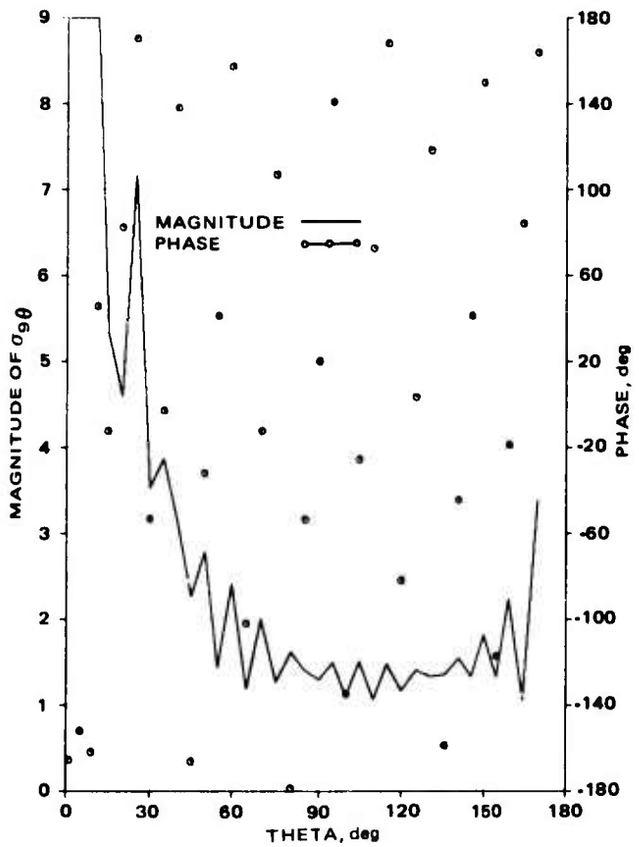

Figure 16. θ-polarized diffraction coefficient, $\sigma_{9\theta}(\theta, \theta_o)$, m = 9.

5.0 COMPUTATION OF MODAL AND TOTAL FIELDS

Modal circumferential fields from the asymptotic approach were computed by summation of the optical, transition, and diffraction fields for the particular mode. The computed patterns of both polarizations were plotted with the corresponding patterns from the exact modal series computer program. The m = 0 modal fields for the θ-polarization are shown in Figure 17. The agreement between the modal series and the asymptotic methods is excellent for this mode for $\theta \geq 15$ degrees; however, for $\theta < 15$ degrees, the asymptotic method computations begin to depart from those of the modal series.

The comparative field patterns for the m = 1 mode for the θ-polarized and φ-polarized field components are shown in Figures 18 and 19, respectively. For this mode, the agreement of the two methods is quite good over most of the θ-range. For the θ-polarization the two patterns differ in the range of $\theta < 20$ degrees. A noticeable difference is also seen in the vicinity of $\theta = \theta_o$, but the agreement is still excellent. The differences between the two different patterns of the φ-polarization occur in the same θ-range as noted previously for the θ-polarization.

As the mode number is increased, the variations between the patterns from the two computation methods become more pronounced. The pattern for the m = 2 mode illustrates these characteristics. For the θ-polarization, Figure 20, the two patterns differ by about 1 dB in the range of $45^o \leq \theta \leq 165^o$. For values of θ outside this range, the difference between the two patterns is greater than for the lower order modes shown previously. Similar differences between the two patterns are also seen in the φ-polarized field. Both of these patterns were computed for the azimuth angle of $\phi = 40$ degrees and are shown in Figure 21. For the φ-polarization, however, the differences between the

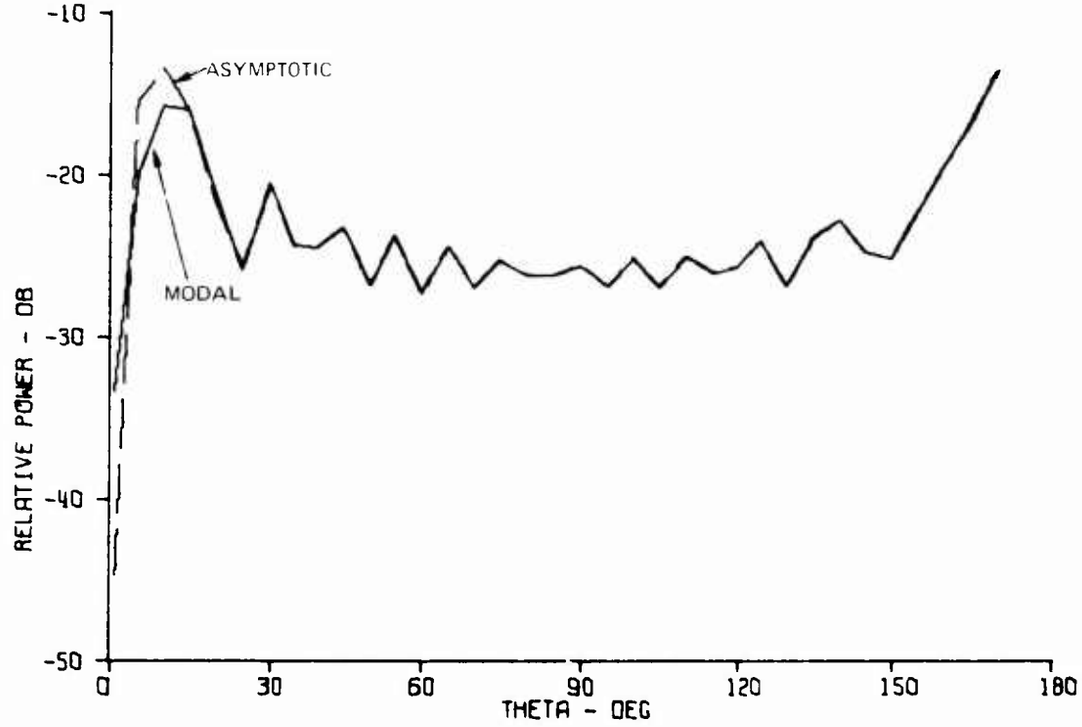

Figure 17. Comparison of modal series solution and asymptotic solution, E_θ, m = 0, $\phi = 0^o$.

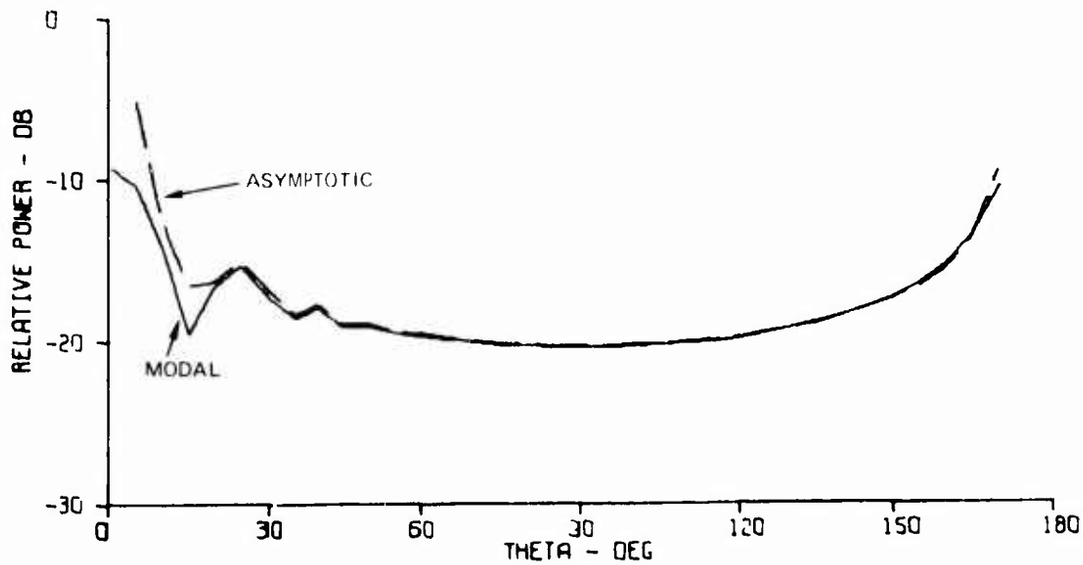

Figure 18. Comparison of modal series solution and asymptotic solution, E_θ, m = 1, $\phi = 0^o$.

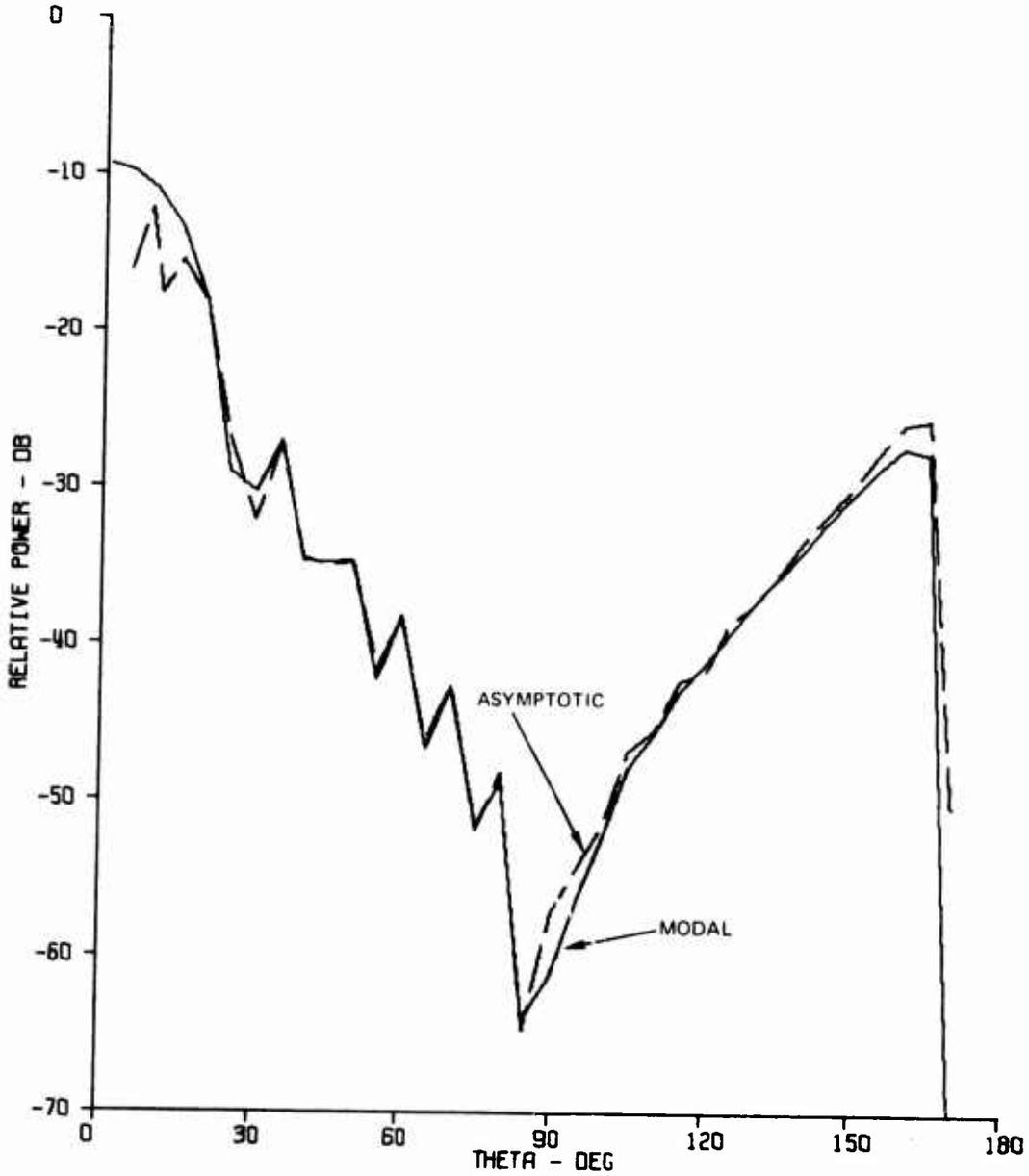

Figure 19. Comparison of modal series solution and asymptotic solution, E_ϕ, $m = 1$, $\phi = 90^o$.

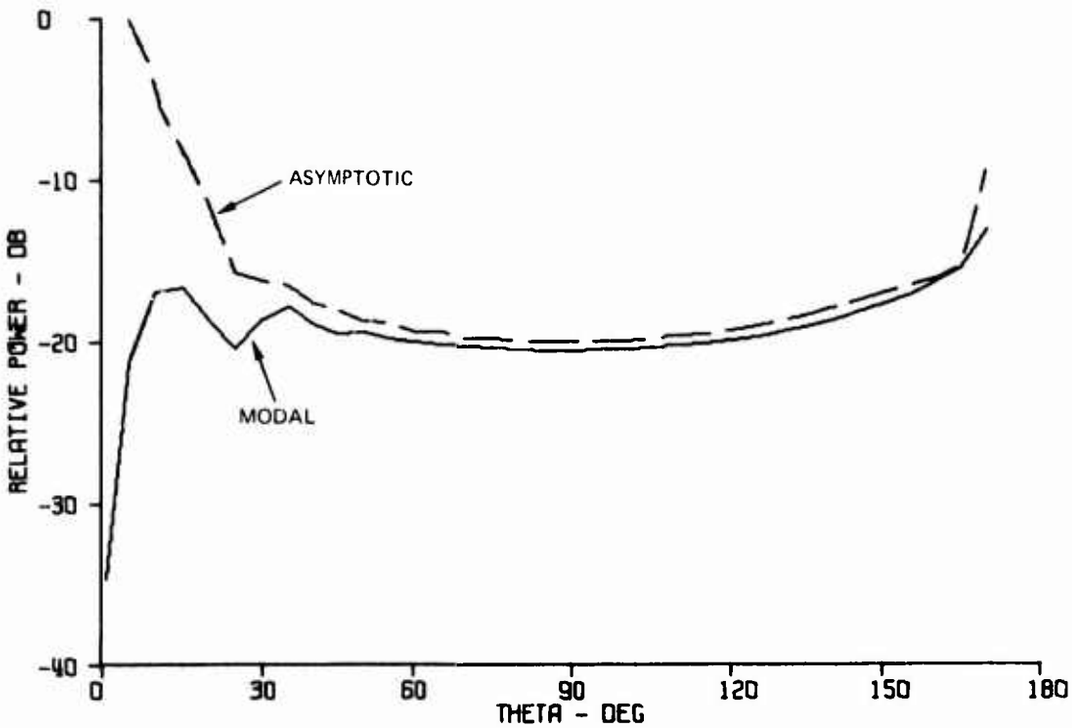

Figure 20. Comparison of modal series solution and asymptotic solution, E_θ, m = 2, $\phi = 0^o$.

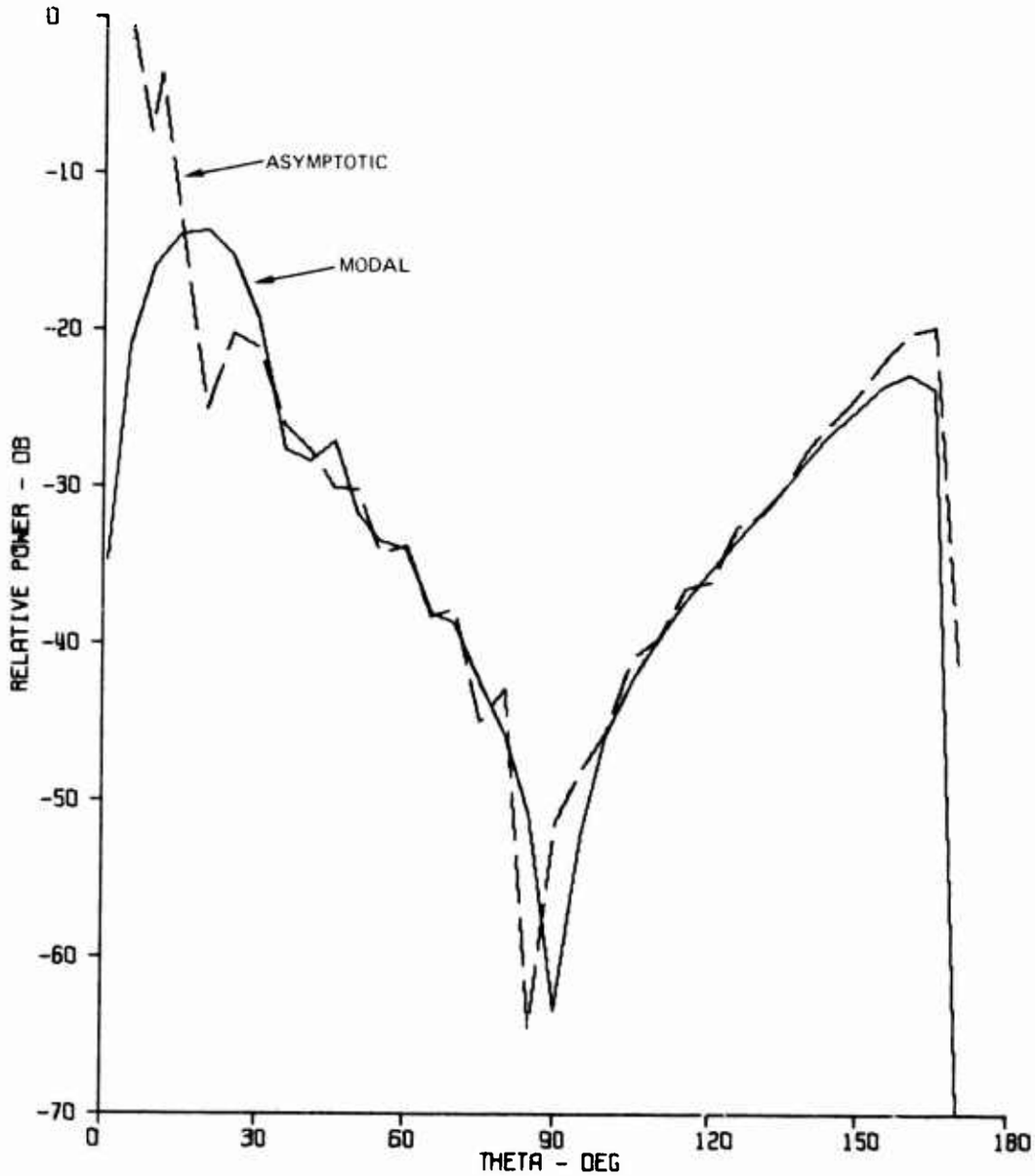

Figure 21. Comparison of modal series solution and asymptotic solution, E_ϕ, m = 2, $\phi = 40^o$.

two patterns extend to values of $\theta < 30$ degrees. Additionally, the null in the broadside region of the asymptotically computed pattern is shifted approximately 5 degrees toward the tip of the cone compared with the pattern from the exact modal series program. Thus, the pattern from the asymptotic method is not accurate in the region $\theta < 30$ degrees.

In the Second Quarterly Report*, an expression of the integral $P_{2\phi Ci}^{(1)(A)}$ was obtained and later used in computation of the total transition field of the ϕ-polarization. The effect of this term on the transition field was discussed in that report. The effect of the same term on the total field, however, is more apparent. Figure 22 shows two total field patterns of the ϕ-polarization for the m = 1 mode. Both patterns include the contribution from the above contour integral. In addition, one of the patterns is the result of 66 terms in the series ΣS_{1n} and ΣS_{2n} while the other pattern was computed with only 39 terms used in the two series. A comparison between the two patterns shows that the broadside region is greatly dependent on the number of terms of the above sums, i.e., the termination of the series. It is evident from Figure 22 that, for proper convergence, care must be taken to use a sufficient number of terms.

A comparison of the pattern of Figure 22 that corresponds to 66 terms in the series and the patterns of Figure 19 shows that the consideration of $P_{2\phi Ci}^{(1)(A)}$ tends to change the pattern significantly at broadside. In fact, the contribution of the contour integral, in effect, shifts the null of the pattern at the broadside region by approximately 10 degrees from the null of the pattern from the modal series. In view of this effect, the $P_{2\phi Ci}^{(1)(A)}$ contour integral should not be included in future computations.

The consideration of the above contour integral, as well as of some other higher order (1/ka) terms, was motivated by the desire to improve the correspondence of the two patterns in Figure 19, particularly in the region 90 to 150 degrees. However, when the modal series pattern for this mode was computed again at closer intervals ($\Delta\theta = 2.5^{\circ}$), the plotted pattern did, in fact, contain certain small oscillations similar to those of the asymptotically

---

*Bargeliotes and Villeneuve, Second Quarterly Report, loc. cit.

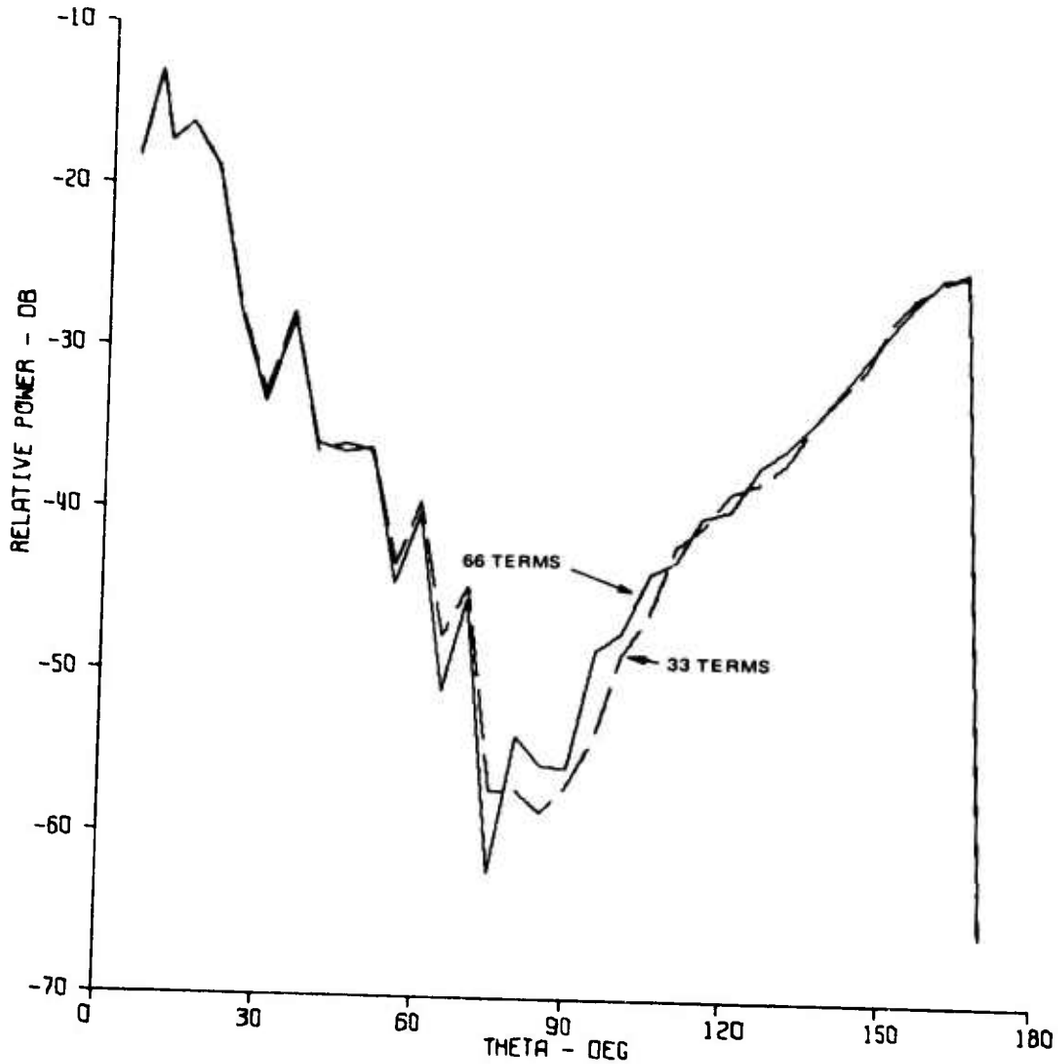

Figure 22. Asymptotic solution with $P_{2\phi Ci}^{(1)(A)}$, 66 and 33 terms in series, E_ϕ, m = 1, $\phi = 90^o$.

computed pattern. The results are shown graphically in Figure 23. Because the two patterns agreed as well as expected for $\theta < 85$ degrees, no additional computations were necessary for this region.

It is pointed out that only those terms of the contour integrals of the E_ϕ expression that are proportional to $(1/ka)^{1/2}$ and $1/\nu_n$ were considered in the computation of the diffraction field and the diffraction coefficients. Consideration of higher order terms in $(1/ka)^{1/2}$, even though of order zero in $1/\nu_n$, would result in ka-dependent $\sigma_{m\phi}(\theta, \theta_o)$, i.e., dependent on the position of the radiating element relative to the cone tip.

The computer program was appropriately modified to allow computation of the diffraction coefficients over the useful range of theta of the asymptotic expressions. For the remaining range of theta, field points were computed by the normal mode series section of the program. After the diffraction coefficients were computed and stored, they were used as input data to the program for subsequent computation of the fields from slots at other locations on the cone. Figure 24 shows the θ-polarized total pattern for the first three modes, M = 2. It also shows the same pattern computed completely by the normal mode series program. The pattern computed from the asymptotic expressions is clearly inaccurate for $\theta < 35^o$; the agreement with the normal mode series computation is quite good over the remaining range of theta except at $\theta = 170^o$. Here, the asymptotic curve is 2.4 dB higher than the normal mode series curve. In view of the behavior of the higher order mode transition and diffraction fields discussed earlier, it is anticipated that total patterns that include higher order modes will differ significantly from corresponding patterns from the normal mode series. The ϕ-polarized total pattern for the first three modes is shown in Figure 25.

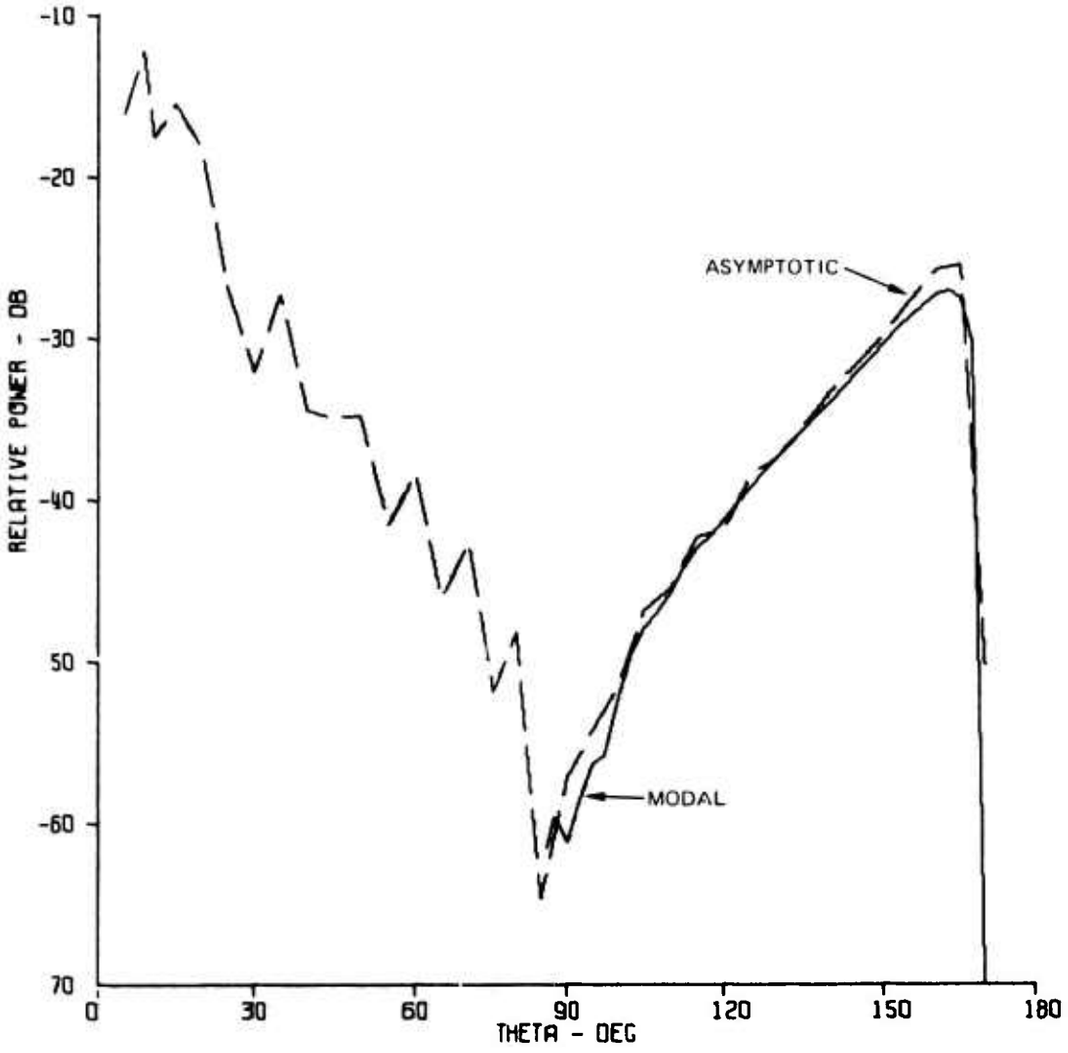

Figure 23. Comparison of modal series solution ($\Delta\theta = 2.5^{o}$) and asymptotic solution, $E\phi$, m = 1, $\phi = 90^{o}$.

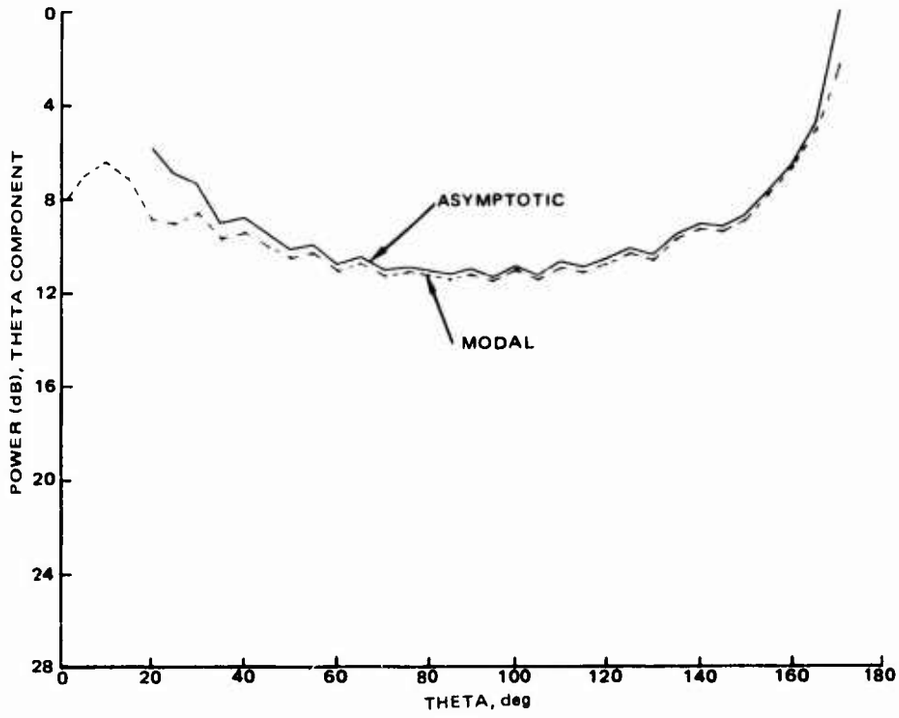

Figure 24. Comparison of modal series solution and asymptotic solution, M = 2, total patterns, E_θ, $\phi = 0^o$.

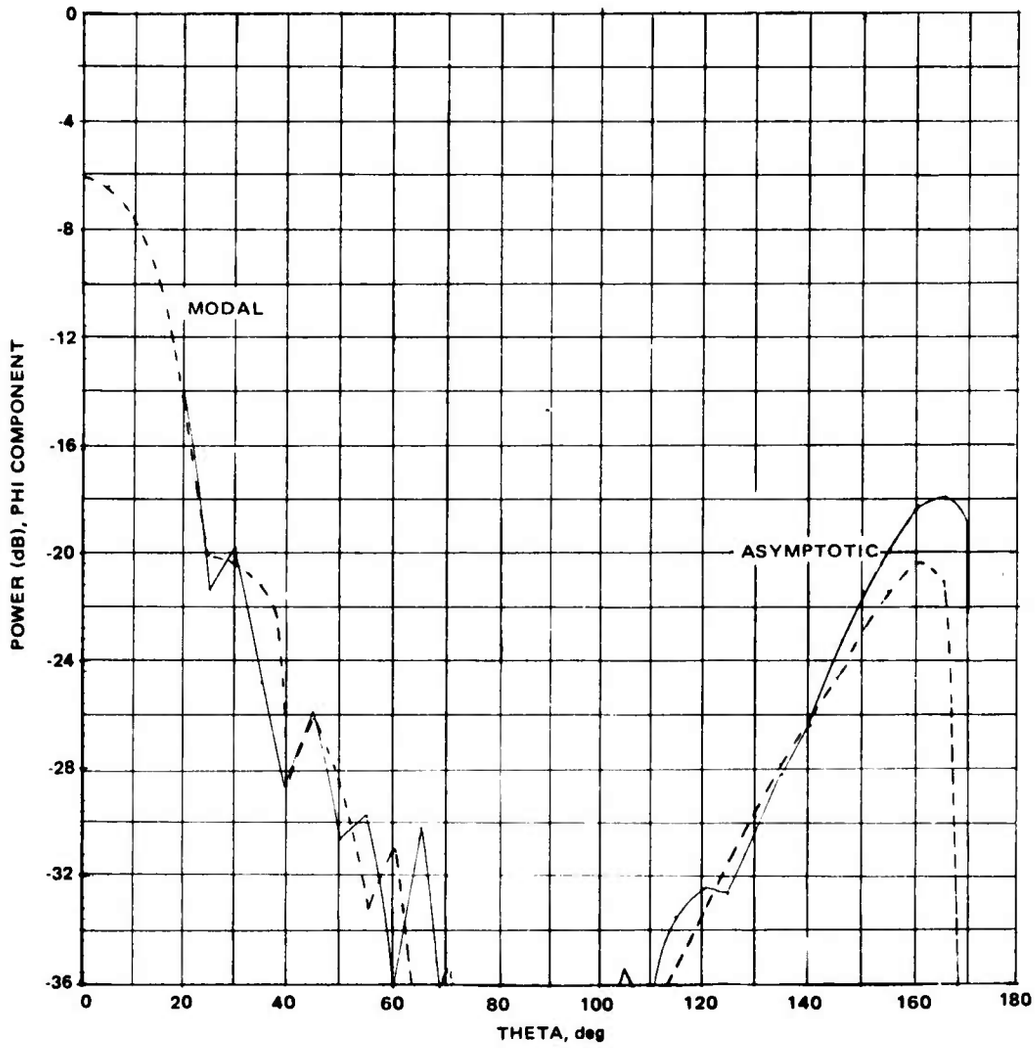

Figure 25. Comparison of modal series solution and asymptotic solution, M = 2, total patterns, E_ϕ, $\phi = 80^\circ$.

6.0 MUTUAL COUPLING COMPUTATIONS

The effect of scattering from the tip on antenna impedance for slots on cones was considered by Golden et al*. The mutual admittance between two slots was approximately calculated with the use of a cylindrical model with the same local radii of curvature as the cone. The equivalent cylinder has a radius equal to the radius of the circular cross section of the cone midway between the two slot antennas.

Mutual coupling computations for circumferential slots on a cylinder were performed with the computer program obtained from Stewart. The program computes self- and mutual admittance of circumferential slots as a function of angular separation for various separations in the radial direction. These mutual coupling computations were utilized to check accuracy of mutual coupling results from the Geometrical Theory of Diffraction approach developed by A. Hessel. The admittance characteristics of two slots for cylinder radii of 1.999 inches and 3.777 inches at frequencies of 9.0 and 9.75 GHz, respectively, are shown in Figures 26 and 27.

---

*K.E. Golden, G.E. Stewart, and D.C. Pridmore-Brown, "Approximation Techniques for the Mutual Admittance of Slot Antennas on Metallic Cones," IEEE Trans. on Antennas and Propagation, Vol. AP-22, January 1974, pp. 43-48.

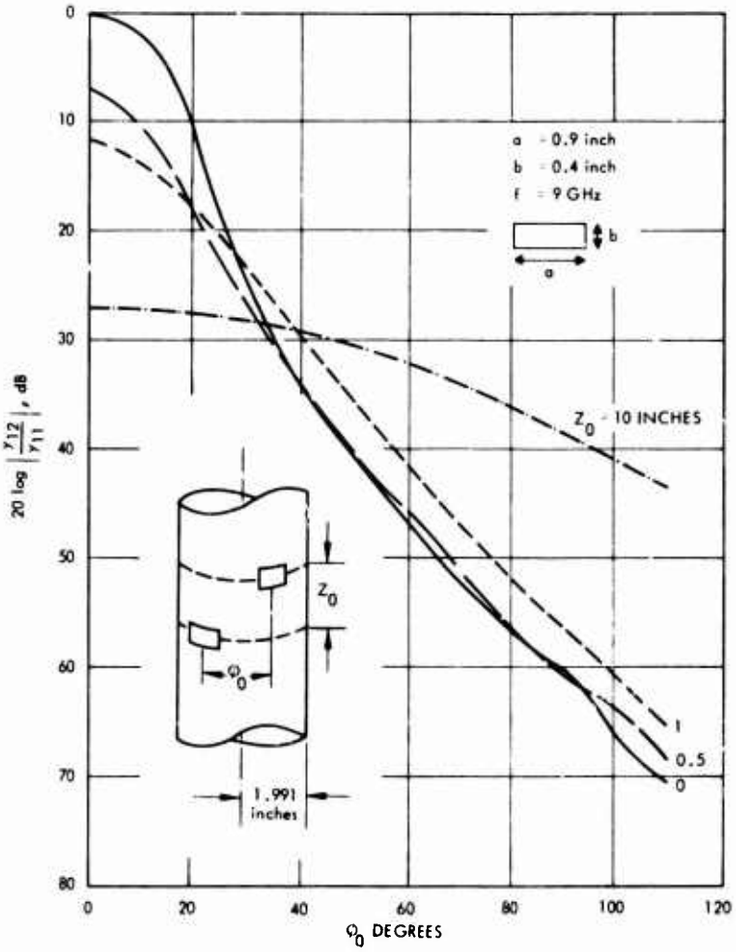

Figure 26. Mutual admittance of circumferential slots on a conducting cylinder, ρ_{in} = 1.991 inch.

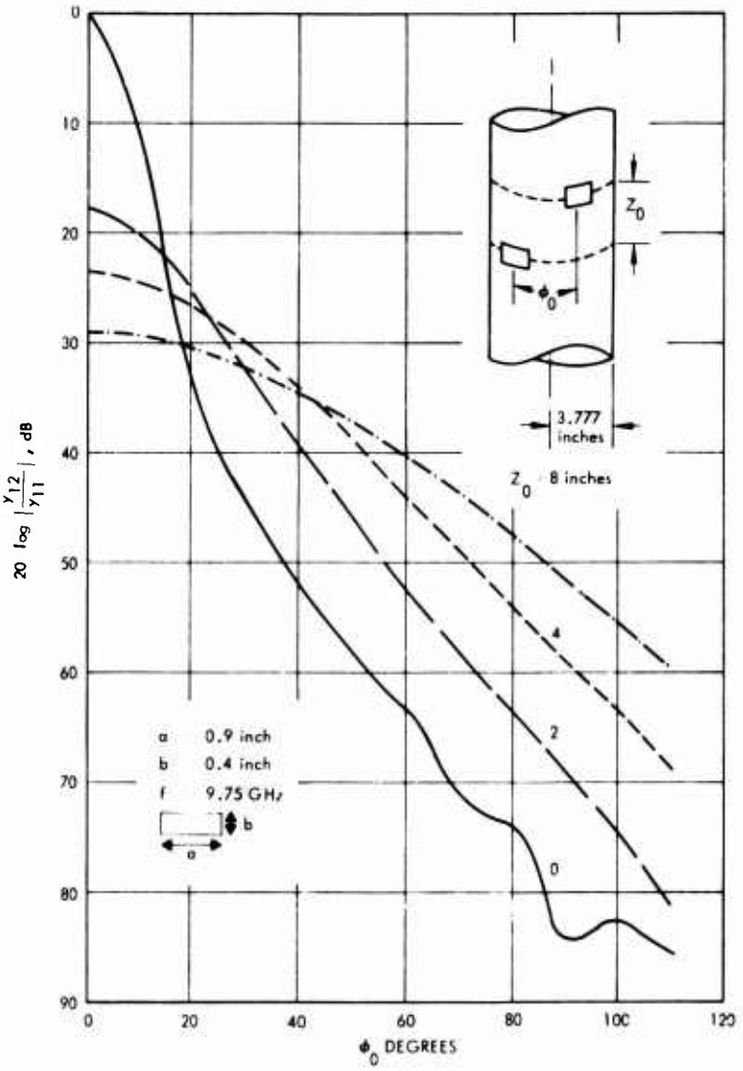

Figure 27. Mutual admittance of circumferential slots on a conducting cylinder, ρ_{in} = 3.777 inch.

7.0 RECOMMENDATIONS FOR FURTHER INVESTIGATIONS

The various terms of the asymptotic expressions representing the E_θ and E_ϕ radiation fields of a slot on a conducting cone will be computed and analyzed in detail. Computations of the diffraction coefficients of the field components were also performed for the lower order modes. The accuracy of the representation of the radiation fields by the asymptotic expressions was examined by computation of the radiation fields for a particular mode and comparison of the results with the corresponding modal fields from the exact modal series computer program. For the lower order modes the two solutions show good agreement everywhere except, as expected, in the vicinity of the region $\theta < \pi - \theta_0$. For the ϕ-polarization, the region of poor performance of the asymptotic solution extends to about $\theta < 30$ degrees for the $m = 1$ mode. For $m > 1$ modes and a slot location of 39 radians from the tip, the agreement between the asymptotic solution and the exact solution is not so good. The departure is believed to be caused by the asymptotic representation of the Legendre functions used in the transition and optical fields as well as in the diffraction coefficients and from a series expansion of their ratios. An improved representation would eliminate this problem; however, no such improved representation is presently available.

It should be noted that, as presently defined, σ_m and $\sigma_{m\phi}$ each have a singularity at $\theta = \pi - \theta_0$. However, there is a compensating singularity in the transition fields so that the total fields remain finite at that angle. It appears that, by combination of the singular terms in the transition fields with the singularity in the tip diffraction coefficients, new diffraction coefficients could be defined that remain finite everywhere and that describe the diffraction due to the tip of the cone. The total tip diffraction could then be obtained by summation over the new σ_m and $\sigma_{m\phi}$, weighted by the corresponding strength of the mth source coefficient. The remainder of the field could be obtained

by the geometric theory of diffraction and the results combined to give the total field valid for large values of ka.

The combination of the complete modal series solution when ka is small and the geometric theory of diffraction with tip-diffraction coefficients when ka is large would provide the capability for pattern calculations for slots at any distance from the cone tip.